Universidade de Aveiro
2019
Departamento de Química

Catarina Alexandra Morais Saraiva

Engenharia de estruturas semelhantes a capilares incorporadas em hidrogéis para cultura de células 3D

Engineering of capillary-like structures embedded in hydrogels for 3D cell culture

Universidade de Aveiro Departamento de Química
2019

Catarina Alexandra Morais Saraiva

Engenharia de estruturas semelhantes a capilares incorporadas em hidrogéis para cultura de células 3D

Engineering of capillary-like structures embedded in hydrogels for 3D cell culture

Dissertação apresentada à Universidade de Aveiro para cumprimento dos requisitos necessários à obtenção do grau de Mestre em Biotecnologia Industrial e Ambiental, realizada sob a orientação científica do Professor Doutor João Filipe Colardelle da Luz Mano, Professor Catedrático do Departamento de Química da Universidade de Aveiro, e do Doutor João Filipe Ramos da Silva Carvalho Borges, Investigador Júnior do Departamento de Química da Universidade de Aveiro.

o júri

presidente

Professora Doutora Luísa Alexandra Seuanes Serafim Martins Leal
Professora Auxiliar do Departamento de Química da Universidade de Aveiro

Doutora Carmen Sofia da Rocha Freire Barros
Investigadora Principal do Departamento de Química da Universidade de Aveiro

Doutor João Filipe Ramos da Silva Carvalho Borges
Investigador Júnior do Departamento de Química da Universidade de Aveiro

agradecimentos

Em primeiro lugar, gostaria de agradecer ao Professor João Mano pela oportunidade de desenvolver este tema, numa área extremamente interessante e adquirir todo este novo conhecimento. Um grande agradecimento ao Doutor João Borges por todo o incansável acompanhamento e orientação durante todo o ano. Gostaria ainda de agradecer a todos os elementos do COMPASS Reseach Group que, direta ou indiretamente, me apoiaram durante este percurso, salientando a Doutora Sónia Patrício, a Doutora Isabel Rial, o Doutor Tiago Correia e o Doutor Vítor Gaspar. Um agradecimento especial ao Tamagno Pesqueira por todo o tempo dedicado às minhas questões e a toda a ajuda. Um obrigado aos meus colegas de mestrado: Flávia, Inês, Marco, Mariana e Tânia por toda a amizade, companhia e humor. A todos os meus amigos pelo carinho demonstrado durante este capítulo da minha vida, muito obrigada. Esta tese foi suportada pelo projeto de IC&DT "SUPRASORT" (PTDC/QUI-OUT/30658/2017, CENTRO-01-0145-FEDER-030658) suportado pelo Programa Operacional Regional do Centro (Centro2020), na sua componente FEDER, e pela Fundação para a Ciência e a Tecnologia (FCT), na sua componente de Orçamento de Estado, assim como pelo projeto ERA-NET MarineBiotech (ERA-MBT) "BLUETEETH" (ERA-MBT/0002/2015) financiado pela FCT ao abrigo do 7º Programa-Quadro de I&DT da União Europeia (Grant Agreement ID: 604814).

Um enorme obrigada aos meus pais por todo o contributo para o meu sucesso, incluindo todas as boleias, e ao meu irmãozinho!

palavras-chave

Polímeros de origem marinha, tecnologia de deposição camada-a-camada, bioimpressão 3D, estruturas semelhantes a capilares, hidrogéis de goma xantana, células endoteliais, engenharia de tecidos.

resumo

Atualmente, o maior desafio em engenharia de tecidos consiste no desenvolvimento de estruturas e aplicação de estratégias que visem mimetizar a complexidade anatómica e celular, assim como a vascularização de tecidos nativos, de forma a manter a viabilidade e funcionalidade das células. A presença de estruturas funcionais à base de vasos sanguíneos é essencial para garantir o fluxo adequado de nutrientes, assim como a difusão de oxigénio em toda a estrutura de suporte, dois requisitos essenciais para manter a viabilidade celular.

Este trabalho teve como objetivo desenvolver um modelo complexo *in vitro* que mimetize a rede vascular nativa. Com esse intuito, membranas multicamadas compreendendo seis bicamadas de quitosana (CHI)/alginato (ALG) e CHI/ALG-RGD (tripéptido de Arginina (R)-Glicina (G)-Ácido aspártico (D) responsável pela adesão de células à matriz extracelular) foram produzidas, *via* tecnologia de deposição camada-a-camada (do inglês *Layer-by-Layer assembly technology*), em estruturas impressas de ALG. As fibras de ALG revestidas com os filmes multicamadas foram embebidas em goma xantana, quimicamente modificada com grupos metacrilatos, de modo a obter uma estrutura de hidrogel mecanicamente robusta após foto-reticulação por ação da luz UV. A liquefação das estruturas impressas de ALG, contendo as multicamadas de CHI/ALG ou CHi/ALG-RGD, com ácido etilenodiamino tetra-acético (EDTA), levou à formação de microcanais nos quais se cultivaram células endoteliais humanas, extraídas da veia umbilical durante 24 horas. Os resultados obtidos demonstraram que os microcanais compreendendo as membranas multicamadas à base de CHI/ALG-RGD contribuíram para uma maior adesão celular, demonstrando o seu potencial para estratégias de engenharia de tecidos e medicina regenerativa.

keywords

Marine origin polymers, layer-by-layer, 3D bioprinting, capillary-like structures, xanthan gum hydrogels, endothelial cells, tissue engineering.

abstract

Nowadays, the biggest challenge in tissue engineering consists in developing structures and in the application of strategies to emulate the anatomical and cellular complexity and vascularization of native tissues to maintain cell viability and functionality. The presence of functional blood vessel networks is essential to ensure adequate nutrient flow and oxygen diffusion throughout the support structure, two key requirements for maintaining cell viability.

This work aimed to develop a complex *in vitro* model that mimics the native vascular network. To this end, a multilayered membrane made of six bilayers of chitosan (CHI)/alginate (ALG) or CHI/ALG-RGD (tripeptide of Arginine (R)-Glycine (G)- Aspartic acid (D) responsible for the cellular adhesion to the extracellular matrix (ECM)) were produced via Layer-by-Layer (LbL) assembly technology on the ALG printed structures. The ALG structures coated with the multilayered membranes were embedded in xanthan gum, chemically modified with methacrylated groups in order to obtain a mechanically robust hydrogel structure after photocrosslinking by UV light exposure. The liquification of the ALG printed structures, coated with the CHI/ALG, CHI/ALG-RGD or without the multilayers membranes, with ethylenediaminetetraacetic acid (EDTA), led to the formation of microchannels in which human umbilical vein endothelial cells (HUVECs) were cultured for 24 hours. The obtained results demonstrate that the microchannels encompassing CHI/ALG-RGD multilayered membranes contributed to a larger cellular adhesion, demonstrating their potential to be applied in tissue engineering and regenerative medicine strategies.

Contents

List of figures

List of tables

Abbreviations

2D – Two-dimensional
3D – Three-dimensional
ALG – Alginate
BM – Basement membrane
CAD – Computer-aided design
CHI – Chitosan
DD – Degree of N-deacetylation
Dil – 1,1'-Dioctadecyl-3,3,3',3'-tetramethylindocarbocyanine perchlorate
EDTA – Ethylenediaminetetraacetic acid
ECs – Endothelial cells
ECM – Extracellular matrix
FN – Fibronectin
GMA – Glycidyl methacrylate
HUVECs – Human umbilical vein endothelial cells
LbL – Layer-by-Layer
LIFT –Laser-induced-forward transfer
PBS – Phosphate buffered saline
PSL – Projection stereolithography
QCM-D – Quartz crystal microbalance with dissipation monitoring
RGD – Arg-Gly-Asp
RITC – Rhodamine B isothiocyanate
SLA – Stereolithography
SMCs – Smooth muscle cells
STL – Standard triangular language
XG – Xanthan gum

Chapter 1 – Motivation

Chapter 1 – Motivation

When an organ fails or disfunctions, it can be due to many reasons. To date, the most common treatment strategies to address such events resort to the use of autografts (transplanting tissues or organs from a healthy site to the injured site in the same patient) and allografts (transplanting tissues or organs from a deceased donor or cadaver to the patient), which, although generally successful, entail major hurdles.[1] For instance, those treatment strategies involve very high costs, chronic pain, possible immunogenicity, several surgeries, anatomical limitations and quite long post-operative recovery, which extensively limit their use. In addition, in case of allografts, there is also the risk of disease transfer, infection or rejection of the organ or tissue to be transplanted from the donor by the patient. All of this implies that thousands of people would have to wait for long periods and could even die while waiting for the suitable functional transplant.[2, 3] Currently, only a low percentage of patients waiting to receive an organ end up finding one available and compatible. As an alternative to the lack of human organs and tissues to study and test, scientists have turned to the use of animal models and two-dimensional (2D) cell-culture to study tissues and organs disfunctions and their reaction to drugs.[1] Although promising, such strategies do not provide an exact representation of the human tissues and organs microenvironment.

2D cell-cultures can develop differently when in three-dimensional environments, diverging in some features like cell-cell and cell-matrix interactions, morphology and interactions. The animal models have been used for years in the pharmaceutical and cosmetic industries as testing subjects for their discoveries. Although very useful for the screening of drug effects and assessment of treatment strategies to get new cures for damaged tissues and organs, some drugs may be harmless to animals and have undesired effects in humans or the opposite can happen.[4]

Along with that and in similarity with 2D cell-culture studies, animal models do not represent truthfully the human tissues and organs. Furthermore, animal models lack the ability to mimic [5] for example, human tumors and drug therapeutic/toxic responses. In this last decade, there has been a visible growth in the protest by the general public against the use of animal models. These opposing voices have been a growing force with a significant financial impact. Hence, tissue engineering has been gathering tremendous attention by the medical and engineering communities as an interdisciplinary field of research that employs

the principles of chemistry, materials science and engineering and biology towards providing astonishing materials and technologies for developing functional biological substitutes of dysfunctional tissues and organs. By designing the tissues and organs to grow, in a personalized fashion, to mimic an individual's original anatomic tissue in their size, shape and immunological compatibility, it is theorized that it will be possible to overcome the lack of compatible organ availability and reduce the probability of infection and/or host immune rejection of the transplants by the patient.[6] The materials used in regenerative strategies need to be able to fully overtake the functions of the original tissue/organ or to stimulate the regeneration of the patients' tissue, in order to have a successful tissue regeneration strategy.

The ideal cellular material for tissue engineering would be stem cells owing to their intrinsic capacity to differentiate in distinct type of cell according to the targeted tissue, the scaffolds should be fabricated by resorting to biocompatible, biodegradable and non-toxic biomaterials, and should exhibit mechanical properties consistent with the anatomical tissue or organ to be repaired. Moreover, stem cells' aptitude of self-renewal can be conserved continuously over generations. However, cells collected from mature (non-stem) cells and 'adult' stem cells (for example mesenchymal stem cells) can also be used up to a certain degree.[7]

As for the scaffold, it may mimic the function of the native extracellular matrix, of the tissue or organ to address. It provides a physical support to cell and may include growth factors and specific ligands in order to trigger an enhanced cellular response, *i.e.* to allow the cells to attach, migrate, proliferate and differentiate. The ideal characteristics for a scaffold to be used in tissue engineering consist in biodegradability, biocompatibility, high porosity and a well-defined 3D structure. The scaffold should also allow for cell-cell interaction due to its importance in the cellular development.[8]

The scaffold's nature is of high importance as its properties have influence over the organization and differentiation of the cells. The use of multilayered films allows for the entrapment in-between layers of bioactive molecules and provides with a physical substrate able to be chemically modified. In this project, we used multilayered membrane, not only to encourage the cells attachment to it but also as a mimicry of the physical barrier the separates the blood from the other organs.

References

1. Leberfinger, A. N., Dinda, S., Wu, Y., Koduru, S. V., Ozbolat, V., Ravnic, D. J., & Ozbolat, I. T. (2019). Bioprinting functional tissues. *Acta Biomaterialia*. https://doi.org/10.1016/J.ACTBIO.2019.01.009
2. Langer; Robert, & Vacanti, J. P. (1993). Tissue engineering. *Science*, *260*(5110), 920–926. https://doi.org/https://www.jstor.org/stable/2885618
3. Dvir, T., Timko, B. P., Kohane, D. S., & Langer, R. (2011). Nanotechnological strategies for engineering complex tissues. *Nature Nanotechnology*, *6*(1), 13–22. https://doi.org/10.1038/nnano.2010.246
4. He, J., Mao, M., Liu, Y., Shao, J., Jin, Z., & Li, D. (2013). Fabrication of nature-inspired microfluidic network for perfusable tissue constructs. *Advanced Healthcare Materials*, *2*(8), 1108–1113. https://doi.org/10.1002/adhm.201200404
5. Derby, B. (2012, November 16). Printing and prototyping of tissues and scaffolds. *Science*. American Association for the Advancement of Science. https://doi.org/10.1126/science.1226340
6. Vats, A., Tolley, N. S., Polak, J. M., & Gough, J. E. (2003). Scaffolds and biomaterials for tissue engineering: A review of clinical applications. *Clinical Otolaryngology and Allied Sciences*, *28*(3), 165–172. https://doi.org/10.1046/j.1365-2273.2003.00686.x
7. Vats, A., Tolley, N. S., Polak, J. M., & Buttery, L. D. K. (2002). Stem cells: sources and applications. *Clinical otolaryngology and allied sciences*, *27*(4), 227–32. https://doi.org/10.1046/j.1365-2273.2002.00579.x
8. Ren, K., Hu, M., Zhang, H., Li, B., Lei, W., Chen, J., Chang, H., Wang, L., & Ji, J. (2019). Layer-by-layer assembly as a robust method to construct extracellular matrix mimic surfaces to modulate cell behavior. *Progress in Polymer Science*. https://doi.org/10.1016/j.progpolymsci.2019.02.004

Chapter 2 – Prevascularization strategies

Chapter 2 – Prevascularization strategies

Tissue engineering seeks to meet the demand for tissues and organs functioning for addressing biomedical and healthcare purposes. However, despite the enormous advances in the field, there are still some issues that prevent its use commercially.[1] One of the major limitations in tissue engineering is the application of strategies to emulate the anatomical and cellular complexity and vascularization of native tissues to maintain cell viability and functionality. The lack of functional vascular networks in engineered tissues has been a struggle for the scientific community since the early developments in the field and represents a great challenge in terms of physiology, immunology, and manufacturing demands.[2–4]

1. The vascular system

The vascular or circulatory system's major function is to provide the circulation of the blood carrying oxygen, nutrients and metabolic byproducts throughout the body, perfusing organs and tissues to maintain cell viability and functionality. Without this network, there are limitations concerning the diffusion of nutrients and oxygen, thereby resulting in restriction of the size of the developed tissues.[5] It is possible to divide this system into two interconnected but distinct systems: the cardiovascular which is responsible for the circulation of the blood and the lymphatic system that oversees the circulation of lymph.

Plasma, erythrocytes, leukocytes, and thrombocytes constitute the blood. Plasma is the extracellular matrix of blood cells where they are also found suspended. Erythrocytes or red blood cells contain hemoglobin bound to oxygen. Leukocytes, also known as white blood cells are responsible for immune response. Thrombocytes, commonly known as platelets has a primary function to clot blood vessel injuries in order to stop the bleeding. All of this is pumped through the body by the beating action of the heart. Lymph, the liquid that flows through lymph capillaries, is formed by the collection of excess liquid produced by the interstices of tissues and gathered in these vessels. After its transport through the lymph nodes, it joins back to the bloodstream.[3]

The blood vessels in conjugation with the heart and the blood vessels form the cardiovascular system. The blood circulates through the body within the blood vessels,

which can be differentiated into three types: arteries, veins, and capillaries. The arteries carry the blood from the heart to the rest of the body and the veins conduct the blood that ran through the body into the heart. The smallest blood vessels in the body are named capillaries and is where the exchange of water, oxygen, nutrients, and other compounds between the blood and the tissues occurs.[1, 6] The arteries are composed of five layers of adventitia, elastic lamina, smooth muscle cells (SMCs), basement membrane (BM), and endothelial cells (ECs). The arteries ramify into arterioles (made of three layers of SMCs, BM, and ECs), metarterioles, and arterial capillaries. The capillaries only have two layers of BM and ECs.[6]

Tissues have a 100-200 μm oxygen, nutrients and waste diffusion limit which restricts the possible dimensions of tissues to bioengineer due to the cells not surviving beyond this limit (Figure 2.1). Within a tissue, cells that distance more the 200 μm from a blood vessel or capillary are not able to receive nutrients and oxygen from it and nor expel their metabolic waste and, as such, they do not survive. Pre-vascularization can be an answer to avoid cellular necrosis for tissues thicker than the diffusion limit by producing structures similar to blood vessels that aim to assure the delivery of oxygen and bioactive molecules to ensure the development of the tissue *in vitro*.[5, 7]

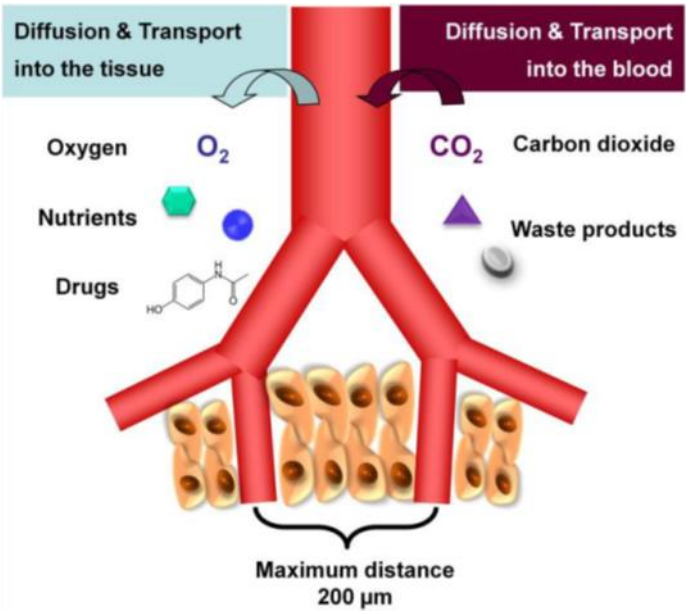

Figure 2.1 – Illustration of the diffusion and transport processes in vascularized tissues *in vivo*. Image obtained from [7].

2. Blood vessel formation and assembly

In embryogenesis, clusters of small dimensions encompassing vascular progenitor cells are formed from the mesoderm layer (angioblasts).[8, 9] The peripheral cells within these clusters differentiate into endothelial cells, while the ones present in the core differentiate into blood cells. This process is termed vasculogenesis. As the cells rearrange, a primary network is formed, and it is initiated the production of proteases with the ability to destroy their surrounding extracellular matrix, allowing the cells to outflow from the network walls and proliferate to form new vessels.[8, 10] Endothelial cells can secrete factors that recruit mural cells which will produce the extracellular matrix. This matrix plays an important role in the stabilization of the new vessels' network. Proceeding angiogenesis is the release of pro-angiogenic factors that direct the migration and sprouting of the endothelial cells. This newly formed vessels grow, proliferate, and interact with already existing vessels via anastomosis.[8, 11]

3. Importance of vascularization

Oxygen is necessary for cells to maintain the cells alive. It reaches the cells via passive diffusion and as a consequence, the oxygenation gradient has a tendency to decline from the peripheral to the core of tissues.[4, 12] In some cases, it is possible that the tissues' core is quite deep that the cells will experience a hypoxic environment. In such environments, the lack of oxygen may lead to cellular apoptosis after prolonged exposure periods *in vivo*. This is a result of the shortage in oxidative phosphorylation and anaerobic respiration.[13] On the other hand, the excess of oxygen or hyperoxia is also detrimental to the cells, possibly leading to decelerating the proliferation of cells in cultures which can also end up leading to cells' apoptosis. As such, it is key to find the right balance in terms of oxygen supply to cells in order to achieve thriving tissues.[12, 14]

In addition to the supply of oxygen and nutrients, and the removal of waste products and toxins, the vascular network itself also plays a significant role on cell proliferation and differentiation. The deficiency in nutrient supply and accumulation of cellular waste can be followed by cell starvation which influences cell development.[15, 16] Adhesion, proliferation, differentiation, and a variety of other cellular functions are dependent on signal transduction and cellular communication, which are, in part, mediated by vasculature structures. The

cardiovascular system is the highway for the response of the immune system. It works in favor of the tissue in cases where potential pathogens encounter immune cells and locating and directing to infection sites. However, especially in transplanting constructs into bodies, the vasculature allows for the immune cells to come in contact with the transplanted construct and recognize it as foreign and elicit an immune response.[3, 12]

Tissue engineered 3D biological structures emerged as a reliable alternative to overcome the lack of organ transplant availability and the high process cost, as well as to reduce the probability of infection and/or host immune rejection of the transplants by the patient. Such shortcomings can be surpassed by designing the tissues and organs to grow in a personalized fashion, aiming to fully recapitulate an individual's original anatomic tissue in terms of the size, shape and immunological compatibility.[17] As such, to engineer functional tissue engineered constructs, there is the need to combine cells, porous scaffolds and suitable bioactive signaling cues, which represent the three pillars of tissue engineering.[18, 19]

4. Interest in prevascularization

Human native tissues have very specific architectures and each tissue possess a unique structural organization. In cases where tissue engineered constructs fail to accurately mimic the heterogeneous nature of native tissues and are implanted in patients, there is the possibility to induce a disease or even to trigger the development of a carcinogenic tissue.[4, 20] Also contributing to the success of an engineered complex tissue is its ability to control the diverse functions of the cells. The lack of such control leads tissue engineered constructs to be dysfunctional and malignant. The matrix stiffness, molecular gradients, and hierarchical structure also influence the viability of the cells within a large engineered tissue construct and, consequently, are obstacles in the path to viable engineered organs.[21] However, one of the main challenges in tissue engineering strategies is the lack of a vascularized structure.

It is possible to promote the vascularization of a construct after implantation. In such cases, the perforated, un-vascularized construct takes advantage of the host's peripheral vascular system capability of angiogenic sprouting. However, it is a rather time-consuming vascularization technique that compromises its use, being possible that the construct's core

reaches necrosis earlier than the formation of a functional vascular network. On the other hand, pursuing prevascularization *in vitro* may accelerate the anastomosis with the host vasculature, enabling the core's viability.[4, 11]

The incorporation of a prevascular network into an engineered tissue before implantation has shown to be vital to the production of larger size and functional tissues and organs that avoid the formation of a necrotic core. Prevascularizing constructs reduces the need for vasculogenic and angiogenic processes after implantation and, in mice, have shown to promote the vascularization and the inosculation with the host's vasculature.[22, 23] Prevascularized engineered tissues have also demonstrated great interest to replace studies using animal models and *ex vivo* (cadaveric) human tissue models.[4]

To date, the vascularization of engineered constructs as shown promising results in thin tissue slides (2D), while the vascularization of 3D constructs has experienced a slow pace development. The most common *in vitro* model still in use is a cell monolayer, also referred to as 2D cell culture.[24] However, in humans, the cells are enclosed within a 3D extracellular matrix. This means that the most used *in vitro* model for scientific studies do not accurately mimic the microenvironment within the human body. The differences between the use of 2D versus 3D platforms include cellular adhesion, proliferation, migration and differentiation. The 3D *in vitro* model replicates more precisely the cellular microenvironment in human tissues.[25–27] However, designing a 3D model entails much more challenges and difficulties. A common undesired occurrence is the loss of cellular viability during long-term culture, which extensively reduces the lifespan of the *in vitro* models. Therefore, researchers have been looking into modifications of the system to improve the long-term cellular viability.[24, 28] The prevascularization of these models has the potential to increase the lifetime of the cellular viability, as well as better emulate the native tissue vasculature. Having a vascular network within an engineered 3D model will have an influence over cell-cell interactions, primarily when using co-culture tissue models.[29, 30] The cell-cell crosstalk influence the cell functionality *in vivo*.[24]

5. Prevascularization approaches

Several techniques have been proposed to date to trigger the formation of a prevascularized structure. The *in vivo* prevascularization involves a porous acellular scaffold that is attached to the side of the patient's artery. The vascularization occurs post-implantation with the cells infiltrating the scaffold through angiogenic sprouting. The next step involves waiting a time period of a few weeks to allow for the development of a microvascular network. The microvascular network is then harvested and explanted to the host's target site.[11] With this process, the scaffold can be perfused after implantation. Nonetheless, two different surgeries are required. In addition, the vascularized construct must be removed from the site of the first surgery and implanted into the ischemic target site. This process can be challenging due to limitations in nutrients that arise after implantation.[31, 32]

In addition, for 3D tissue constructs of bigger dimensions, the already time-consuming process would require even more time. It is possible that this time period is too long and, consequently, lead to necrosis prior to the formation of a vascular network. To avoid this fate, the interest in prevascularization has gathered plenty of attention among the scientific community. The possibility of having a tissue that is vascularized prior to its implantation is desired as it speeds up the process of anastomosis with host vasculature in order to allow the cells to have faster access to nutrient supply.[3, 7] Currently, there are several methods being used to fabricate blood vessels-like structures *in vitro*, as described in the following sections.

5.1. Bioprinting

3D bioprinting has grown rapidly in the last decade due to the intrinsic capability to produce biological constructs, differentiating itself from traditional 3D printing mainly due to the materials used.[33] The traditional 3D printing consists in accurately create 3D constructs in an additive manufacturing/layer-by-layer (LbL) fashion using a heated nozzle to melt plastic.[34, 35] The term bioprinting is used when referring to additive manufacturing techniques that fabricate living tissue constructs from a biological ink (or bioink). 3D bioprinting (Figure 2.2) is used to print tissue-like structures and scaffolds inspired by the

biological structure and organization of the native tissues to mimic while controlling their size, internal structure and materials to be assembled. [36–38] In addition, 3D bioprinting allows the combination of scalability, resolution, and repeatability, in opposition to techniques such as direct laser ablation or electrostatic discharge.[39–41]

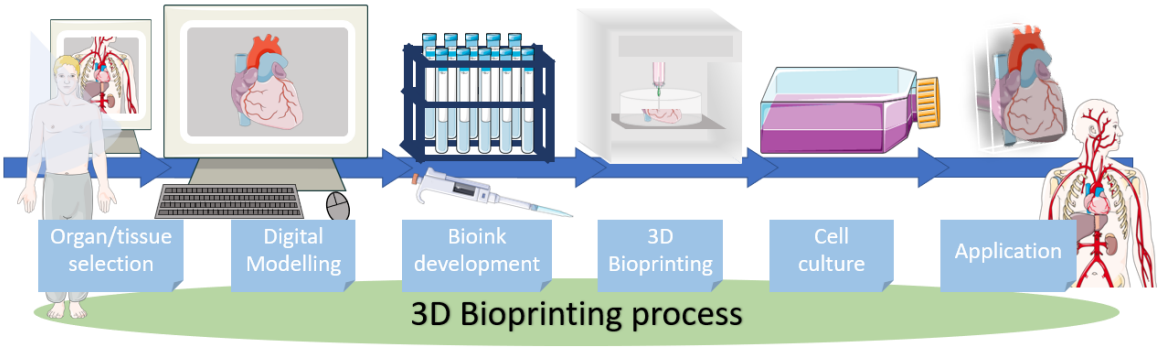

Figure 2.2 – Schematic illustration of the 3D bioprinting process: Starting in the selection of the intended tissue/organ to bioprint, CT scanning/MRI technique or other 3D scanning techniques are used to transfer a digital copy of the organ/tissue into a modeling software. In digital form, the tissue/organ can be structurally modified if needed and then processed in a digital modeling software with the goal to generate a G-code. The selection of the optimal materials to be used as bioink is based on the constructs' application. Then, the biomaterials are prepared for the bioprinting step, in which a 3D bioplotter is used to obtain a 3D construct. After bioprinting, some constructs may need some incubation time before its application either on medical cases, such as implantation or in laboratory cases, for example in drug testing.

The bioprinting techniques are divided by their dependence on fundamentally different principals. As such it is possible to categorize them as extrusion, ink-jet, and laser-based approaches.[42] The field of bioprinting has gathered a lot of attention, with researchers not only striving to improve the performance of already existing bioprinters but also to develop new bioprinting technologies. An example is the development of the "freeform reversible embedding of suspended hydrogels" process (Figure 2.3) which allows the fabrication of 3D constructs that possess a complex architecture not achieved utilizing conventional approaches.[43]

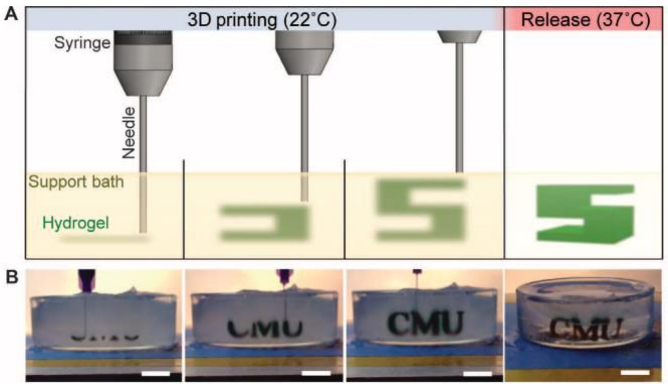

Figure 2.3 – Freeform reversible embedding of suspended hydrogels method performed by Hilton and co-workers by extruding ink into a thermoreversible support bath. **A)** Schematic representation of the process. B) Letters printed in alginate with the freeform reversible embedding of suspended hydrogels method in a gelatin support bath. The apparent deformation of the letters in the last photograph is due to change in optical properties, convective currents and the diffusion of the black dye out of the alginate. Scale bars: 1 cm. Image adapted from [43].

Nowadays, the bioprinters commercially available have features that allow the user to control features such as temperature and viscosity to pursue groundbreaking studies. This has provided the ability to fabricate hybrid constructs composed of multiple hydrogel materials and cell types, meaning control over mechanical stiffness and composition of the construct.[44] An example, is the bioprinting of scaffold-free, large-diameter tubular tissue constructs using an indirect agarose molding technique (Figure 2.4).[41] This technique provides the researchers with control over the tube's shape, dimension and hierarchical branching. Another application of this approach is the fabrication of toroid-shaped, scaffold-free tissue from an alginate-based mold obtained from bioprinting, showing the possibility to design and produce viable tissue with customizable architecture.[45, 46]

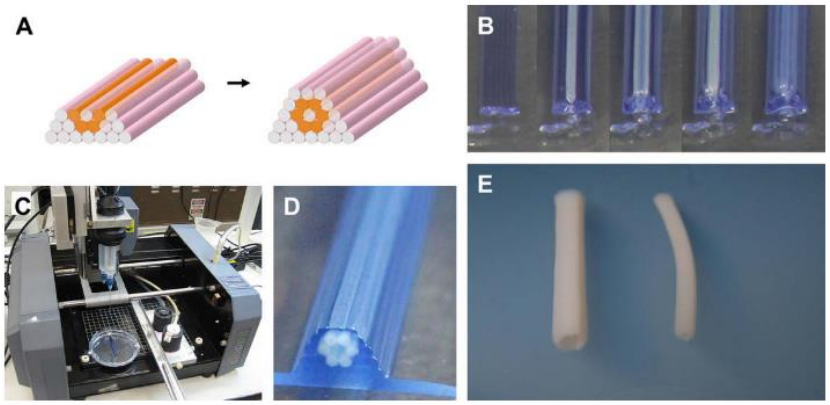

Figure 2.4 – Bioprinting of large diameter tubular tissue constructs. A) Template design; B) Deposition of

agarose cylinders (stained with blue dye); C) Bioprinter used; D) Bioprinted result. E) Difference in diameters obtained 3 days post-printing. Image obtained from [41].

More recently, laser-based bioprinting approaches have been introduced, which include the Laser-Induced-Forward-Transfer (LIFT) technique and stereolithography (SLA). The LIFT technique consists of focusing the beam of a highly powered laser onto a photo-absorbent material coated with a bioink. When this material is hit with enough laser intensity, it vaporizes causing high-pressure zone. The increase of pressure propels a small quantity of the bioink onto a glass slide, which aims to collect the ink.[46–48]

Laser-assisted bioprinting has several advantages, including the ability to print a high density of cells with high-resolution, as well as the use of bioinks disclosing high viscosity. Furthermore, it can be used at room temperature, print single cells within scaffolds and is a non-contact printing method, which means that it does not cause mechanical damage to the cells. However, it is a time-consuming methodology and the side effects of the lasers in the cells are not yet fully understood. Moreover, this technology has limitations in the number of layers that can be printed, therefore limiting its application in tissue engineering strategies.[35, 36]

SLA was patented in the 1980s despite being only in the last couple of decades that was able to be applied in the tissue engineering field by demonstrating the intrinsic capability to encapsulate cells and fabricate 3D tissue scaffolds. Projection stereolithography (PSL) can fabricate living tissue constructs with controllable porous architecture. The porous scaffolds demonstrate better cellular viability when compared to their non-porous counterparts, mostly due to nutrient delivery within the scaffolds.[18, 49]

Currently, the SLA systems commercially available have been modified in order to expand their use in tissue engineering such as the ability to produce 3D constructs composed of different layers made of different cell types and material composition, aiming to improve the long-term viability of encapsulated cells.[34, 50]

A key advantage of the bioprinting technology is the ability to obtain truly 3D perfusable microchannel networks with the possibility to be lined with ECs. To study the effects of the vascular network spatial organization, the most useful approaches are 3D networks fabricated into pre-designed patterns (Figure 2.5).[42] It has been observed that human umbilical vein endothelial cells (HUVECs) are capable of lining the lumen in microchannels embedded in hydrogels after their extrusion-based bioprinting.[51] To achieve

this network, the channels were bioprinted within the bulk ECM using fugitive ink (also known as sacrificial ink), that was later on removed. This resulted in microchannels seeded with HUVECs. In another study, it was demonstrated the possibility to print cell-laden tubular hydrogel constructs using a multilayered coaxial extrusion system, which demonstrated cell viability, tunable tube dimensions, perfusability and complex architecture.[52]

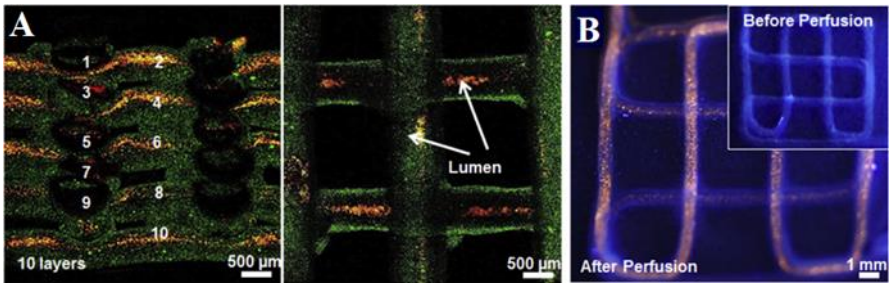

Figure 2.5 – B) Confocal micrographs showing the 3D structure of 10 layers of tubes with green fluorescent beads, which were perfused with red fluorescent microbeads inside the lumens. Scale bars: 500 µm. **C)** Confocal micrographs showing the before and after the injection of red fluorescent microbeads into single, continuous bioprinted tube. Scale bar: 1 mm. Image adapted from [52].

Although 3D bioprinting has shown a lot of promise in fabricating vasculatures, it still has several drawbacks. It is important to consider the biocompatibility of the sacrificial ink, as well as the removal process to use and the resulting by-products. For instance, some sacrificial inks may contain cytotoxic compounds harmful to cell viability and may even affect cell phenotype. The same issues can occur in the fugitive ink removal processes which require its chemical dissolution and heat treatment.[53, 54]

3D bioprinting technologies are widely known for the possibility to fabricate objects with complex architecture. Nevertheless, the bioprinted material is usually soft with a high water content, even when it has incorporated live cells incorporated, which restricts the level of structural complexity possible to be achieved in the printed constructs.[53, 55]

5.2. Microfluidics (Lithography)

Microfluidic technology has grown in popularity in a vast array of fields, particularly for achieving vascularization of tissue constructs. With microfluidics it is possible to fabricate complex microfluidic networks with ultra-high resolution, providing control over the geometrical features of the network. One approach for the vascularization of tissue constructs is to fabricate microchannel networks within bulk collagen matrix and posteriorly seed these channels with HUVECs to simulate perfusable blood vessels.[56] Another approach encompass the fabrication of microchannel networks in agarose hydrogels encapsulating murine fibroblasts. While these channels were not seeded with HUVECs, it is possible to demonstrate an increase in the murine fibroblast viability by the perfusion of the hydrogel with microchannels.[57]

Another approach to vascularization is to provide supplemented medium under controlled flow rate and direction to ECs within the hydrogel device, fabricated using microfluidic technology. The cells spontaneously self-assemble into perfusable vascular networks within the hydrogel.[58] The vascular networks obtained from the self-assembly of the ECs is considered to be the result of natural vasculogenic and angiogenic processes and the vessels have a higher rate of formation using microfluidic technologies.[59] However, the vascular networks engineered by microfluidics are restricted to a thin tissue (unlike the networks obtained via the bioprinting) differing from the 3D organization found in the human native vascularized tissues. Additionally, the vascular networks are not able to be easily removed from the microfluidic system for implantation, thus reducing the possibility to be applied in regenerative medicine.[58, 59]

5.3. Micropatterning

The approach to vascularization by micropatterning consists of patterning biological material on a substrate aiming to induce vasculogenesis with controlled spatial organization or patterning directly onto adhesive substrates. Micropatterning techniques used for vascular applications include soft lithography and laser-assisted micropatterning. One approach is to fabricate PDMS stamps by resorting to standard photolithographic techniques (Figure 2.6). The stamps can be used to pattern fibronectin strips on glass coverslips which show preferential adhesion from the human endothelial progenitor cells (hEPCs) in comparison to

non-adhesive poly(ethylene glycol) (PEG) surface.[60]

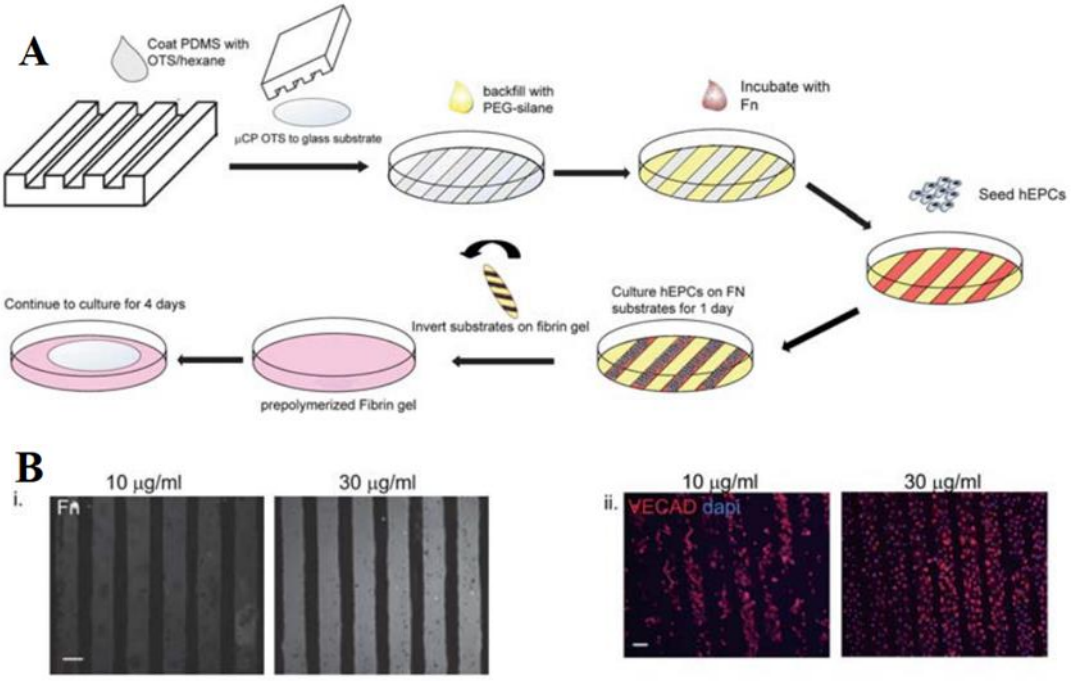

Figure 2.6 – A) Schematic representation of the fabrication of the stamps used to pattern the fibronectin strips. B) **i.** fluorescence microscopy images of fluorescently -labeled fibronectin in an array of 100 μm stripes on a polyethylene glycol silane coated glass. Scale bar: 100 μm **ii.** Human endothelial progenitor cells (stained with mouse anti-human vascular endothelial cadherin (red) and nuclei (blue)) spread and adhesion, 24 hours after seeding. Both adhesion and distribution are higher on the condition with higher concentration of fibronectin. Scale bar: 100 μm. Image adapted from [60].

Another approach consists in the production of substrates with design-specific microgrooves that are possible to be filled with cells after *in vitro* cell culture. With this technique it is possible to fabricate lumenized vascular tubes where the user can control their diameters by varying the dimensions of their microgrooves. These lumenized channels were observed to branch into multiple tubes whilst preserving their lumenized structure when the cellular material was previously cultured within the branched microgrooves of varying designs. The result consists in lumenized endothelial tubes with controlled spatial organization.[61]

Micropatterning allows for vascular networks to be harvested and encapsulated within a hydrogel to produce vascularized tissue later used for *in vivo* implantation. Nevertheless, its throughput still needs optimization in addition to achieve a 3D vascularized tissue.[62]

5.4. Wire molding

Immediate perfusion of medium throughout the engineered tissue is feasible by incorporating microchannels within the tissue construct. A common fabrication procedure used in wire molding is the submersion of a wire within a pre-polymer solution, which can have cells. The wire is manually removed after polymerization, leaving behind a microchannel.[63] An advantage of this approach is the possibility to distribute equal microchannels throughout large tissue constructs and within various *Z*-planes, thus engineering tissues in a true 3D form.[64] As mentioned above, the vasculature present in the human body often present more complex architectures than a monolayer of ECs. Combining wire molding with other procedures has been reported to recapitulate the bilayer structure *in vitro* that mimics the one found in capillaries, *i.e*. a layer of ECs surrounded by a layer of a smooth muscle cell (SMC).[65]

Besides the immediate perfusability, the wire molding approach is advantageous due to the precise control over the microvascular diameter. Moreover, the fact that this approach can vascularize thick 3D constructs is also advantageous when compared with other approaches that are limited to thin sheets of tissue.

5.5. Cell sheet engineering

When using cell sheet technologies, a confluent monolayer of cells is formed being able to be harvested. Usually, they are obtained via culture in thermo-responsive polymers as they can be detached without resorting to chemical treatment. After harvesting, the cells in the sheets remain viable. One approach to vascularization comprises stacking cell sheets of ECs and fibroblasts in varying configurations. When vascular networks were formed, these constructs were implanted and demonstrated enhanced vasculogenesis.[4, 55, 66]

The major strengths of cell sheet engineering technology rely on the nature of the scaffold material used, the obtained cell density and harvesting method. The ECM is naturally produced by the cells which disregard the need for sacrificial biocompatible materials and cytotoxic chemicals. Sheets with high cell density and homogenous cell distribution can contribute for a higher regenerative function. The detaching and stacking of the sheets may require some thermal treatment, however due to its low level, it does not

cause significant harm to the cells. Another advantage is the possibility to create thick stackings and to control the vascular network's orientation.[66]

6. Conclusion

To have available engineered tissues and organs raises expectations in optimizing organ supply for transplants as well as in bettering clinical trials with more precise organ representations.

To date, successfully engineered tissue constructs already in clinical use consist in avascular tissues. With 2D models having proven their success, 3D thick functional vascular models have remained intangible. Ideally, the perfect engineered vascularized constructs should mimic the hierarchical order of the vascular network. The ability to fabricate accurate replicas of human native vascular networks *in vitro* is now the focus of several research endeavors. It is being increasingly recognized that in order to successfully engineer large tissues and organs, including micro-scale capillary networks, it is key to maintain the viability of large cell populations within thick constructs.

The aforementioned highlighted techniques are just a few that have great potential to trigger *in vitro* vascularization. Each of them, with their own strengths and weaknesses, focuses in a different path towards achieving the same goal. To be able to engineer functional tissues and organs ready for implantation largely depends on the presence of mature and well-perfused vascular networks, which is not a short-term goal but still a deep field to discover.

The bioprinting technologies have undergone a recent boost in scientific research. Currently, different approaches using bioprinting technologies allow to 3D bioprint multicellular constructs with high precision, with an organization similar to native tissues, as well to fabricate perfusable 3D microchannel networks within the bulk tissue. Bioprinting is a relatively new technology when compared with others such as photolithography, meaning its development is still in its infancy and, thus, has plenty of room for improvements.

7. References

1. Khademhosseini, A., & Langer, R. (2016). A decade of progress in tissue engineering. *Nature Protocols*, *11*(10), 1775–1781. https://doi.org/10.1038/nprot.2016.123
2. Datta, P., Barui, A., Wu, Y., Ozbolat, V., Moncal, K. K., & Ozbolat, I. T. (2018). Essential steps in bioprinting: From pre- to post-bioprinting. *Biotechnology Advances*, *36*(5), 1481–1504. https://doi.org/10.1016/j.biotechadv.2018.06.003
3. Sharma, D., Ross, D., Wang, G., Jia, W., Kirkpatrick, S. J., & Zhao, F. (2019). Upgrading prevascularization in tissue engineering: A review of strategies for promoting highly organized microvascular network formation. *Acta Biomaterialia*. https://doi.org/10.1016/j.actbio.2019.03.016
4. Liew, A. W. L., & Zhang, Y. (2017). In vitro pre-vascularization strategies for tissue engineered constructs-bioprinting and others. *International Journal of Bioprinting*, *3*(1), 3–17. https://doi.org/10.18063/IJB.2017.01.008
5. Gershlak, J. R., Hernandez, S., Fontana, G., Perreault, L. R., Hansen, K. J., Larson, S. A., Binder, B. Y. K., Dolivo, D. M., Yang, T., Domiko, T., Rolle, M. W., Weathers, P. J., Medina-Bolivar, F., Cramer, C. L., Murphy, W. L., & Gaudette, G. R. (2017). Crossing kingdoms: Using decellularized plants as perfusable tissue engineering scaffolds. *Biomaterials*, *125*, 13–22. https://doi.org/10.1016/J.BIOMATERIALS.2017.02.011
6. Chen, D. X. B. (2019). *Bioprinting Vascular Networks in Scaffolds. In: Extrusion Bioprinting of Scaffolds for Tissue Engineering Applications*. Springer, Cham. https://doi.org/10.1007/978-3-030-03460-3_7
7. Novosel, E. C., Kleinhans, C., & Kluger, P. J. (2011). Vascularization is the key challenge in tissue engineering. *Advanced Drug Delivery Reviews*, *63*(4), 300–311. https://doi.org/10.1016/j.addr.2011.03.004
8. Haase, K., & Kamm, R. D. (2017, April 1). Advances in on-chip vascularization. *Regenerative Medicine*. Future Medicine Ltd. https://doi.org/10.2217/rme-2016-0152
9. Boyce, S. T., & Lalley, A. L. (n.d.). Tissue engineering of skin and regenerative medicine for wound care. https://doi.org/10.1186/s41038-017-0103-y
10. Peak, C. W., Singh, A., Gaharwar, A. K., Peak, C., Cross, L., Singh, A., & Gaharwar, A. K. (2016). Microscale Technologies for Engineering Complex Tissue Structures. https://doi.org/10.1007/978-3-319-20726-1_1
11. Zhang, W., Wray, L. S., Rnjak-Kovacina, J., Xu, L., Zou, D., Wang, S., Zhang, M., Dong, J.,

Li, G., Kaplan, D. L., & Jiang, X. (2015). Vascularization of hollow channel-modified porous silk scaffolds with endothelial cells for tissue regeneration. *Biomaterials*, *56*, 68–77. https://doi.org/10.1016/j.biomaterials.2015.03.053

12. Rademakers, T., Horvath, J. M., Blitterswijk, C. A., & LaPointe, V. L. S. (2019). Oxygen and nutrient delivery in tissue engineering: Approaches to graft vascularization. *Journal of Tissue Engineering and Regenerative Medicine*. https://doi.org/10.1002/term.2932

13. Das, R., Jahr, H., van Osch, G. J. V. M., & Farrell, E. (2010). The role of hypoxia in bone marrow-derived mesenchymal stem cells: considerations for regenerative medicine approaches. *Tissue engineering. Part B, Reviews*. https://doi.org/10.1089/ten.teb.2009.0296

14. Mach, W. J., Thimmesch, A. R., Pierce, J. T., & Pierce, J. D. (2011). Consequences of Hyperoxia and the Toxicity of Oxygen in the Lung. *Nursing Research and Practice*, *2011*, 1–7. https://doi.org/10.1155/2011/260482

15. Cavallucci, V., Fidaleo, M., & Pani, G. (2016, November 1). Neural Stem Cells and Nutrients: Poised Between Quiescence and Exhaustion. *Trends in Endocrinology and Metabolism*. Elsevier Inc. https://doi.org/10.1016/j.tem.2016.06.007

16. Sthijns, M. M. J. P. E., van Blitterswijk, C. A., & LaPointe, V. L. S. (2018). Redox regulation in regenerative medicine and tissue engineering: The paradox of oxygen. *Journal of tissue engineering and regenerative medicine*, *12*(10), 2013–2020. https://doi.org/10.1002/term.2730

17. Vats, A., Tolley, N. S., Polak, J. M., & Gough, J. E. (2003). Scaffolds and biomaterials for tissue engineering: A review of clinical applications. *Clinical Otolaryngology and Allied Sciences*, *28*(3), 165–172. https://doi.org/10.1046/j.1365-2273.2003.00686.x

18. Bittner, S. M., Guo, J. L., Melchiorri, A., & Mikos, A. G. (2018). Three-dimensional printing of multilayered tissue engineering scaffolds. *Materials Today*, *21*(8), 861–874. https://doi.org/10.1016/j.mattod.2018.02.006

19. Lovett, M., Lee, K., Edwards, A., & Kaplan, D. L. (2009). Vascularization Strategies for Tissue Engineering. *Tissue Engineering Part B: Reviews*, *15*(3), 353–370. https://doi.org/10.1089/ten.teb.2009.0085

20. Schmeichel, K. L., & Bissell, M. J. (2003, June 15). Modelling tissue-specific signaling and organ function in three dimensions. *Journal of Cell Science*. https://doi.org/10.1242/jcs.00503

21. Griffith, L. G., & Swartz, M. A. (2006, March). Capturing complex 3D tissue physiology in vitro. *Nature Reviews Molecular Cell Biology*. https://doi.org/10.1038/nrm1858

22. Baranski, J. D., Chaturvedi, R. R., Stevens, K. R., Eyckmans, J., Carvalho, B., Solorzano, R. D., Yang, M. T., Miller, J. S., Bhatia, S. N., & Chen, C. S. (2013). Geometric control of vascular networks to enhance engineered tissue integration and function. *Proceedings of the National Academy of Sciences of the United States of America*, *110*(19), 7586–7591. https://doi.org/10.1073/pnas.1217796110

23. Auger, F. A., Gibot, L., & Lacroix, D. (2013). The Pivotal Role of Vascularization in Tissue Engineering. *Annual Review of Biomedical Engineering*, *15*, 177–200. https://doi.org/10.1146/annurev-bioeng-071812-152428

24. Elliott, N. T., & Yuan, F. (2011). A review of three-dimensional in vitro tissue models for drug discovery and transport studies. *Journal of Pharmaceutical Sciences*. John Wiley and Sons Inc. https://doi.org/10.1002/jps.22257

25. Naito, H., Yoshimura, M., Mizuno, T., Takasawa, S., Tojo, T., & Taniguchi, S. (2013). The advantages of three-dimensional culture in a collagen hydrogel for stem cell differentiation. *Journal of Biomedical Materials Research Part A*, *101*(10), 2838–2845. https://doi.org/10.1002/jbm.a.34578

26. Soucy, P. A., & Romer, L. H. (2009). Endothelial cell adhesion, signaling, and morphogenesis in fibroblast-derived matrix. *Matrix Biology*, *28*(5), 273–283. https://doi.org/10.1016/j.matbio.2009.04.005

27. Baker, B. M., & Chen, C. S. (2012, July 1). Deconstructing the third dimension-how 3D culture microenvironments alter cellular cues. *Journal of Cell Science*. https://doi.org/10.1242/jcs.079509

28. Burke, A. S., MacMillan-Crow, L. A., & Hinson, J. A. (2010). The Hepatocyte Suspension Assay Is Superior to the Cultured Hepatocyte Assay for Determining Mechanisms of Acetaminophen Hepatotoxicity Relevant to *in Vivo* Toxicity. *Chemical Research in Toxicology*, *23*(12), 1855–1858. https://doi.org/10.1021/tx1003744

29. Mandrycky, C., Wang, Z., Kim, K., & Kim, D. H. (2016). 3D bioprinting for engineering complex tissues. *Biotechnology Advances*, *34*(4), 422–434. https://doi.org/10.1016/j.biotechadv.2015.12.011

30. Giwa, S., Lewis, J. K., Alvarez, L., Langer, R., Roth, A. E., Church, G. M., Markmann, J. F., Sachs, D. H., Chandraker, A., Wertheim, J. A., Rothblatt, M., Boyden, E. S., Eidbo, E., Lee, W. P. A., Pomahac, B., Brandacher, G., Weinstock, D. M., Elliott, G., Nelson, D., Acker, J. P., Uygun, K., Schmalz, B., Weegman, B. P., Tocchio, A., Fahy, G. M., Storey, K. B., Rubinsky, B., Bischof, J., Elliott, J. A.W., Woodruff, T. K., Morris, G. J. Demirci, U.,

Brockbank, K. G.M., Woods, E. J., Ben, R. N., Baust, J. G., Gao, D., Fuller, B., Rabin, Y., Kravitz, D. C., Taylor, M. J., & Toner, M. (2017, June 7). The promise of organ and tissue preservation to transform medicine. *Nature Biotechnology*. Nature Publishing Group. https://doi.org/10.1038/nbt.3889

31. Rouwkema, J., Rivron, N. C., & van Blitterswijk, C. A. (2008). Vascularization in tissue engineering. *Trends in Biotechnology*, *26*(8), 434–441. https://doi.org/10.1016/j.tibtech.2008.04.009

32. Rivron, N. C., Liu, J., Rouwkema, J., de Bouer, J., & Blitterswijk, C. A. van. (2008). ENGINEERING VASCULARISED TISSUES IN VITRO. *NC Rivron et al. European Cells and Materials*, *15*, 27–40. https://doi.org/10.22203/eCM.v015a03

33. Matai, I., Kaur, G., Seyedsalehi, A., McClinton, A., & Laurencin, C. T. (2020, January 1). Progress in 3D bioprinting technology for tissue/organ regenerative engineering. *Biomaterials*. Elsevier Ltd. https://doi.org/10.1016/j.biomaterials.2019.119536

34. Ma, J., Wang, Y., & Liu, J. (2018). Bioprinting of 3D tissues/organs combined with microfluidics. *RSC Advances*. Royal Society of Chemistry. https://doi.org/10.1039/c8ra03022g

35. Zhang, B., Luo, Y., Ma, L., Gao, L., Li, Y., Xue, Q., Yang, H., & Cui, Z. (2018, March 1). 3D bioprinting: an emerging technology full of opportunities and challenges. *Bio-Design and Manufacturing*. Springer. https://doi.org/10.1007/s42242-018-0004-3

36. Pati, F., Gantelius, J., & Svahn, H. A. (2016). 3D Bioprinting of Tissue/Organ Models. *Angewandte Chemie - International Edition*, *55*(15), 4650–4665. https://doi.org/10.1002/anie.201505062

37. Huang, J. H., Kim, J., Agrawal, N., Sudarsan, A. P., Maxim, J. E., Jayaraman, A., & Ugaz, V. M. (2009). Rapid fabrication of bio-inspired 3D microfluidic vascular networks. *Advanced Materials*, *21*(35), 3567–3571. https://doi.org/10.1002/adma.200900584

38. Wu, W., Deconinck, A., & Lewis, J. A. (2011). Omnidirectional printing of 3D microvascular networks. *Advanced Materials*, *23*(24). https://doi.org/10.1002/adma.201004625

39. Xia, C., & Fang, N. X. (2009). 3D microfabricated bioreactor with capillaries. *Biomedical Microdevices*, *11*(6), 1309–1315. https://doi.org/10.1007/s10544-009-9350-4

40. Lim, D., Kamotani, Y., Cho, B., Mazumder, J., & Takayama, S. (2003). Fabrication of microfluidic mixers and artificial vasculatures using a high-brightness diode-pumped Nd:YAG laser direct write method. *Lab on a Chip*, *3*(4), 318–323. https://doi.org/10.1039/b308452c

41. Norotte, C., Marga, F. S., Niklason, L. E., & Forgacs, G. (2009). Scaffold-free vascular tissue engineering using bioprinting. *Biomaterials*, *30*(30), 5910–5917. https://doi.org/10.1016/j.biomaterials.2009.06.034

42. Dababneh, A. B., & Ozbolat, I. T. (2014). Bioprinting Technology: A Current State-of-the-Art Review. *Journal of Manufacturing Science and Engineering, Transactions of the ASME*, *136*(6). https://doi.org/10.1115/1.4028512

43. Hinton, T. J., Jallerat, Q., Palchesko, R. N., Park, J. H., Grodzicki, M. S., Shue, H. J., Ramadan, M. H., Hudson, A. R., & Feinberg, A. W. (2015). Three-dimensional printing of complex biological structures by freeform reversible embedding of suspended hydrogels. *Science Advances*, *1*(9). https://doi.org/10.1126/sciadv.1500758

44. Schuurman, W., Khristov, V., Pot, M. W., Van Weeren, P. R., Dhert, W. J. A., & Malda, J. (2011). Bioprinting of hybrid tissue constructs with tailorable mechanical properties. *Biofabrication*, *3*(2). https://doi.org/10.1088/1758-5082/3/2/021001

45. Tan, Y., Richards, D. J., Trusk, T. C., Visconti, R. P., Yost, M. J., Kindy, M. S., Drake, Christopher J., Argraves, W. S., Markwald, R. R., & Mei, Y. (2014). 3D printing facilitated scaffold-free tissue unit fabrication. *Biofabrication*, *6*(2). https://doi.org/10.1088/1758-5082/6/2/024111

46. Ozbolat, I. T., & Yu, Y. (2013). Bioprinting toward organ fabrication: Challenges and future trends. *IEEE Transactions on Biomedical Engineering*, *60*(3), 691–699. https://doi.org/10.1109/TBME.2013.2243912

47. Odde, D. J., & Renn, M. J. (1999). Laser-guided direct writing for applications in biotechnology. *Trends in Biotechnology*, *17*(10), 385–389. https://doi.org/10.1016/S0167-7799(99)01355-4

48. Lepowsky, E., Muradoglu, M., & Tasoglu, S. (2018). Towards preserving post-printing cell viability and improving the resolution: Past, present, and future of 3D bioprinting theory. *Bioprinting*, *11*(July), 1–17. https://doi.org/10.1016/j.bprint.2018.e00034

49. Lin, H., Zhang, D., Alexander, P. G., Yang, G., Tan, J., Cheng, A. W. M., & Tuan, R. S. (2013). Application of visible light-based projection stereolithography for live cell-scaffold fabrication with designed architecture. *Biomaterials*, *34*(2), 331–339. https://doi.org/10.1016/j.biomaterials.2012.09.048

50. Chan, V., Zorlutuna, P., Jeong, J. H., Kong, H., & Bashir, R. (2010). Three-dimensional photopatterning of hydrogels using stereolithography for long-term cell encapsulation. *Lab on a Chip*, *10*(16), 2062–2070. https://doi.org/10.1039/c004285d

51. Kolesky, D. B., Truby, R. L., Gladman, A. S., Busbee, T. A., Homan, K. A., & Lewis, J. A. (2014). 3D Bioprinting of Vascularized, Heterogeneous Cell-Laden Tissue Constructs. *Advanced Materials*, *26*(19), 3124–3130. https://doi.org/10.1002/adma.201305506

52. Jia, W., Gungor-Ozkerim, P. S., Zhang, Y. S., Yue, K., Zhu, K., Liu, W., Pi, Q., Byambaa, B., Dokmeci, M. R., Shin, S. R., & Khademhosseini, A. (2016). Direct 3D bioprinting of perfusable vascular constructs using a blend bioink. *Biomaterials*, *106*, 58–68. https://doi.org/10.1016/j.biomaterials.2016.07.038

53. Gungor-Ozkerim, P. S., Inci, I., Zhang, Y. S., Khademhosseini, A., & Dokmeci, M. R. (2018). Bioinks for 3D bioprinting: An overview. *Biomaterials Science*, *6*(5), 915–946. https://doi.org/10.1039/c7bm00765e

54. Valot, L., Martinez, J., Mehdi, A., & Subra, G. (2019). Chemical insights into bioinks for 3D printing. *Chemical Society Reviews*. https://doi.org/10.1039/C7CS00718C

55. Sarker, M. D., Naghieh, S., Sharma, N. K., & Chen, X. (2018). 3D biofabrication of vascular networks for tissue regeneration: A report on recent advances. *Journal of Pharmaceutical Analysis*, *8*(5), 277–296. https://doi.org/10.1016/j.jpha.2018.08.005

56. Zheng, Y., Chen, J., Craven, M., Choi, N. W., Totorica, S., Diaz-Santana, A., Kermani, P., Hempstead, B., Fischbach-Teschl, C., López, J. A., & Stroock, A. D. (2012). In vitro microvessels for the study of angiogenesis and thrombosis. *Proceedings of the National Academy of Sciences of the United States of America*, *109*(24), 9342–9347. https://doi.org/10.1073/pnas.1201240109

57. Tocchio, A., Tamplenizza, M., Martello, F., Gerges, I., Rossi, E., Argentiere, S., Rodighiero, S., Zhao, W., Milani, P., & Lenardi, C. (2015). Versatile fabrication of vascularizable scaffolds for large tissue engineering in bioreactor. *Biomaterials*, *45*, 124–131. https://doi.org/10.1016/j.biomaterials.2014.12.031

58. Moya, M. L., Hsu, Y. H., Lee, A. P., Christopher, C. W. H., & George, S. C. (2013). In vitro perfused human capillary networks. *Tissue Engineering - Part C: Methods*, *19*(9), 730–737. https://doi.org/10.1089/ten.tec.2012.0430

59. Jakab, K., Norotte, C., Marga, F., Murphy, K., Vunjak-Novakovic, G., & Forgacs, G. (2010). Tissue engineering by self-assembly and bio-printing of living cells. *Biofabrication*, *2*(2). https://doi.org/10.1088/1758-5082/2/2/022001

60. Dickinson, L. E., Moura, M. E., & Gerecht, S. (2010). Guiding endothelial progenitor cell tube formation using patterned fibronectin surfaces. *Soft Matter*, *6*(20), 5109–5119. https://doi.org/10.1039/c0sm00233j

61. Raghavan, S., Nelson, C. M., Baranski, J. D., Lim, E., & Chen, C. S. (2010). Geometrically controlled endothelial tubulogenesis in micropatterned gels. *Tissue Engineering - Part A*, *16*(7), 2255–2263. https://doi.org/10.1089/ten.tea.2009.0584

62. Chaturvedi, R. R., Stevens, K. R., Solorzano, R. D., Schwartz, R. E., Eyckmans, J., Baranski, J. D., … Chen, C. S. (2015). Patterning vascular networks in vivo for tissue engineering applications. *Tissue Engineering - Part C: Methods*, *21*(5), 509–517. https://doi.org/10.1089/ten.tec.2014.0258

63. Nichol, J. W., Koshy, S. T., Bae, H., Hwang, C. M., Yamanlar, S., & Khademhosseini, A. (2010). Cell-laden microengineered gelatin methacrylate hydrogels. *Biomaterials*, *31*(21), 5536–5544. https://doi.org/10.1016/j.biomaterials.2010.03.064

64. Yao, L., de Ruiter, G. C. W., Wang, H., Knight, A. M., Spinner, R. J., Yaszemski, M. J., Windebank, A. J., & Pandit, A. (2010). Controlling dispersion of axonal regeneration using a multichannel collagen nerve conduit. *Biomaterials*, *31*(22), 5789–5797. https://doi.org/10.1016/j.biomaterials.2010.03.081

65. Yoshida, H., Matsusaki, M., & Akashi, M. (2013). Biomedical Applications: Multilayered Blood Capillary Analogs in Biodegradable Hydrogels for In Vitro Drug Permeability Assays (Adv. Funct. Mater. 14/2013). *Advanced Functional Materials*, *23*(14), 1730–1730. https://doi.org/10.1002/adfm.201370069

66. Sakaguchi, K., Shimizu, T., & Okano, T. (2015). Construction of three-dimensional vascularized cardiac tissue with cell sheet engineering. *Journal of Controlled Release*, *205*, 83–88. https://doi.org/10.1016/j.jconrel.2014.12.016

Chapter 3 – Materials and methods

Chapter 3 – Materials and methods

1. Materials

1.1. Alginate

Alginate (ALG, pK_a ~ 3.38 or 3.65 for mannuronic or guluronic acid resides, respectively, M_w = 538 kDa, viscosity ≈250 cP) is a naturally-occurring and hydrophilic polysaccharide, typically extracted from brown algae (*Phaeophyceae*), including *Laminaria digitata*, *Laminaria hyperborea*, *Ascophyllum nodosum*, and *Macrocystis pyrifera*.[1] It has been shown to be very appealing for biomedical and biotechnological applications owing to its biocompatibility, low or even non-toxicity, non-immunogenic properties, low cost, and ionic gelling ability in the presence of divalent cations (*e.g.*, Ca^{2+}, Mg^{2+}, Ba^{2+}) under mild temperature and pH condition.[2, 3] Moreover, owing to its anionic character at pH higher than the pK_a, it allows the build-up of electrostatic-based multilayered systems with oppositely charged cationic polymers.

ALG is a linear binary compound containing blocks of (1–4)-linked β-*D*-mannuronic (M) and α-*L*-guluronic (G) acid residues in its chemical structure.[4–6] The ALG blocks are composed of homopolymeric regions encompassing consecutive M residues, consecutive G residues, and heteropolymeric regions of alternating M and G residues (Figure 3.1). Depending on the species of algae from which ALG is extracted using aqueous alkali solutions, most commonly NaOH, and on the collection period, the ALG's G and M content, sequence, length of each residue, and molecular weight may differ.

The ALG used in this work was acquired from Sigma-Aldrich and used as received, *i.e.* without any further purification.

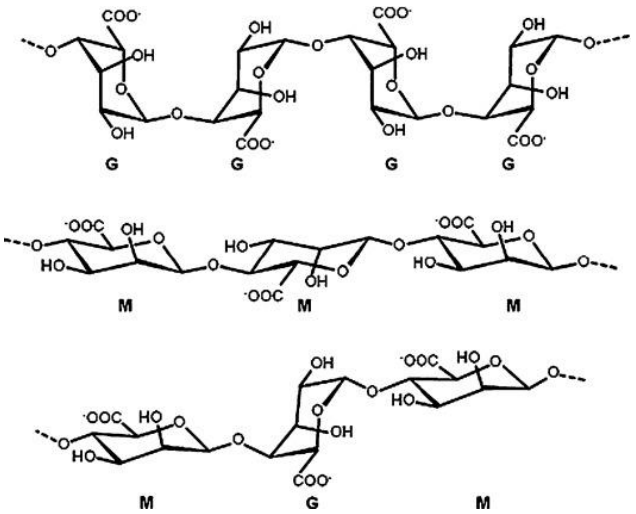

Figure 3.1 – Chemical structure of ALG showcasing the G-block, M-block, and alternating GM-blocks. Image obtained from [3].

1.2. Chitosan

Chitosan (CHI, pK_a ~6-6.5) is an hydrophilic and cationic polysaccharide obtained by the partial deacetylation of chitin, the second most abundant polysaccharide in nature, found mainly in crustaceans' exoskeleton, such as in the crab and shrimp's shells.[7] It presents a linear backbone structure encompassing randomly distributed β-(1–4)-linked *D*-glucosamine and *N*-acetyl-*D*-glucosamine linked through glycosidic bonds (Figure 3.2). CHI has been gathering much attention in biomedical and biotechnological applications owing to its biocompatibility, biodegradability, and antibacterial properties. Moreover, the protonation of its amine groups at pH<pK_a, reveals CHI's polycationic character, making it a highly suitable candidate for the assembly of electrostatically-driven multilayer assemblies for tissue engineering and regenerative medicine strategies.[8, 9]

Chitosan (M_w = 236.8 kDa, 80% degree of deacetylation (DD), viscosity 200−800 cP) was obtained from Primex EHF, that is a recognized Icelandic marine biotechnology company and a leader in the manufacture and supply of pure chitin and CHI biopolymers extracted from the cold water shrimps of Siglufjordur, Iceland.

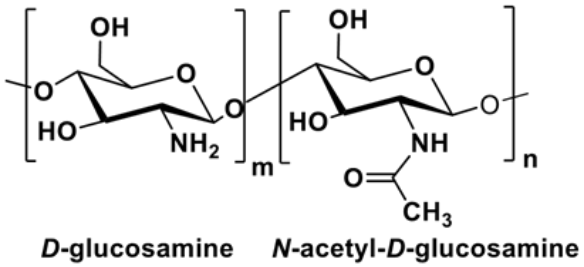

Figure 3.2 – Molecular structure of chitosan.

1.3. Xanthan gum

Xanthan gum (XG) is a water soluble, naturally-occurring exopolysaccharide produced by the bacterial fermentation of glucose, mainly by the Gram-negative bacteria *Xanthomonas campestris*. XG is the most important microbial polysaccharide. Since its approval by the FDA in 1969 as a nontoxic and safe biopolymer, and due to its rheological properties, *i.e.* shear thinning behavior, it has been widely used in the food and pharmaceutical industry, and cosmetics as a thickener and stabilizer.[10, 11] XG chemical structure consists of a primary structure of repeated pentasaccharide units encompassing two glucose units, two mannose units, and one glucuronic acid unit (Figure 3.3). XG backbone comprises a linear (1→4)-linked β-*D*-glucose repeating chain, attached to a charged trisaccharide sidechain composed of *D*-mannose (β-1,4), *D*-glucuronic acid (β-1,2), and *D*-mannose, which are attached to alternate glucose units in the backbone by α-1,3 linkages. The side chain is responsible for assigning the anionic character of XG. Its molecular weight ranges from 2×10^6 to 20×10^6 Da.[10–12]

XG was obtained from the commercial store Celeiro (Doves Farm Foods Ltd, distributed by Bricer Unipessoal, Portugal).

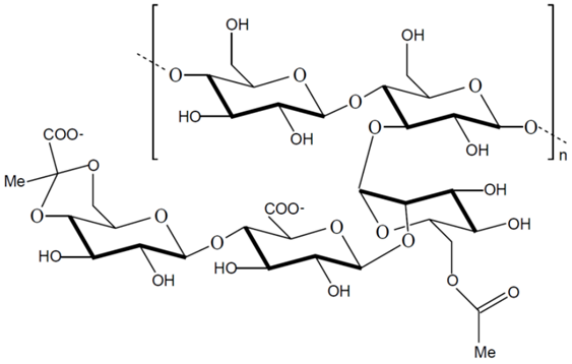

Figure 3.3 – Chemical structure of XG. Image adapted from [12].

2. Methods

2.1. Preparation of the alginate ink

The preparation of the ink followed the method described by Freeman & Kelly, with minor changes in the viscosity of the ink.[2]

Briefly, an ALG ink solution was prepared at 5% (w/v) in phosphate buffer solution (PBS, Sigma Aldrich). Moreover, a 60 mM calcium chloride ($CaCl_2$) aqueous solution was also prepared. To form the desired ALG ink, the aforementioned solutions were mixed up at a volumetric ratio (v/v) of 25:9 (ALG solution: $CaCl_2$ solution). The resulting ALG inks were left to crosslink for 30 minutes prior to the printing process.

2.2. 3D printing using alginate ink

The designed structures were generated using Computer-Aided Design (CAD) software. Each structure was then sliced into layers depending on its height. In this case, there was the need to print solely one layer to form the 3D structure. A 3D Cellink Inkredible bioprinter (Cellink, Sweden) and a 23G (0.33 mm of inner diameter) needle were used to print the ALG structures.

2.3. 3D modelling using CAD

The scaffold was designed using the Blender software. The overall design of the scaffold consisted on a cylinder with a diameter of 0.33 mm (Figure 3.4a), to match the internal diameter of the needle used. The cylinder's length varied between 1 to 5 cm.

Moreover, a sinusoidal shape (Figure 3.4b), a star (Figure 3.4c) and a rough sketch of a capillary representation (Figure 3.4d) were also printed. The CAD designs were saved as Standard Triangular Language (.STL) file extension.

2.4. Printing using Repetier-Host

The obtained .STL files were assembled onto Repetier-Host, a software provided by Cellink company. The printing settings used were: extrusion pressure between 45 to 55 kPa and needle speed of 25 mm/s. All the printing was performed at room temperature. The extrusion pressure, which was set on the Repetier-Host 3D printer had to be constantly optimized during the printing process as the ALG and $CaCl_2$ were in the cartridge. The speed used was the lowest possible to achieve more control over the precision of the printable structure.

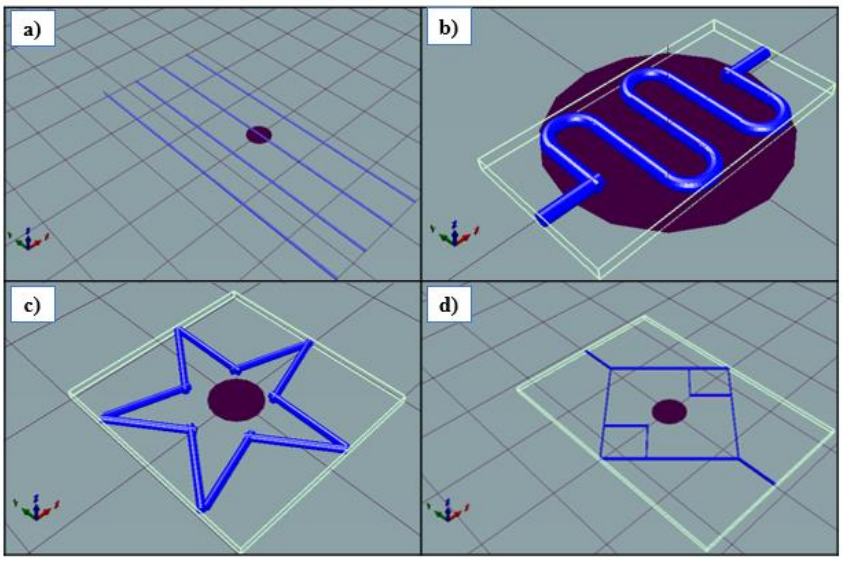

Figure 3.4 – Scaffold design viewed in Repetier-Host: a) cylinder; b) sinusoidal; c) star; and d) capillary representations.

Prior to the printing, the 3D bioprinter was calibrated in the *x*, *y*, and *z* axes. Then, the previously ink loaded cartridges were fitted with the needle tip of choice and placed into the printer's cartridge holder. After 30 minutes of ink pre-crosslinking time, the printing process was started. The designs were printed on a petri dish. Afterwards, the printed structures were immersed in a 60 mM $CaCl_2$ aqueous solution for 5 to 10 minutes to further crosslink the structure. Finally, all the structures were rinsed with deionized water.

2.5. Production of chitosan-alginate multilayered films

2.5.1. Quartz crystal microbalance with dissipation monitoring

The build-up of the CHI/ALG and the CHI/ALG-RGD was monitored *in situ* by quartz crystal microbalance with dissipation monitoring (QCM-D, Q-Sense Pro, Biolin Scientific, Sweden) in a liquid environment. This apparatus measures in real time the frequency and dissipation changes (Δf and ΔD, respectively) of the quartz crystal generated by the adsorption of the polyelectrolyte on the gold-coated 5 MHz AT-cut quartz crystal sensors (QSX301 Gold, Q-Sense, Sweden). The gold-coated quartz crystal substrates were excited at multiple overtones (1, 3, 5, 7, 9, and 11, corresponding to 5, 15, 25, 35, 45, and 55 MHz, respectively). Before testing on the CHI and ALG or ALG-RGD aqueous solutions, the crystals were thoroughly cleaned and then placed in the QCM-D chamber, and equilibrated in an aqueous solution at pH 5 until a baseline was reached. All the experiments were performed at 25°C. The sample's aqueous solutions were prepared at pH 5 and injected with a constant flow rate of 50 µL/min. The CHI solution (0.5 mg/mL) was injected for 6 min. It was followed by the rinsing step that consisted in the injection of deionized H_2O at pH 5 for 4 min, aiming to remove weakly adsorbed layers. In the next step, the solutions used were ALG or ALG-RGD (both at 0.5 mg/mL) and their injection was performed for 6 min. To close the cycle of build-up of one bilayer, another rising step was for 4 min. Multilayered thin films encompassing 6 CHI/ALG and 6 CHI/ALG-RGD bilayers were attempted. The final multilayered thin films were dried under a soft stream of N_2. The frequency of each overtone was normalized to the fundamental resonant frequency of the quartz crystal substrate ($\Delta f_n/n$, in which n denotes the overtone number).

2.5.2. Multilayered membranes build-up

The build-up of the CHI/ALG and CHI/ALG-RGD multilayered membranes on the ALG-based cylindrical and sinusoidal printed structures was performed using an automatic home-made dipping robot (CORPUS®), following the assembling conditions gathered in the QCM-D experiments. The automatic dipping robot allowed us to control the CHI and ALG deposition time, rinsing time, as well the number of cycles, *i.e.* multilayered film thickness.

Briefly, the ALG structures were alternately dipped in the aqueous solutions of the CHI and ALG biopolymers at pH 5 for 6 min each. In-between the immersion of the structures in the CHI and ALG or CHI and ALG-RGD aqueous solutions, washing steps (4 min each) were needed to remove weakly adsorbed molecules and avoid the cross-contamination of the biopolymer solutions. The polyelectrolyte solutions were prepared at a concentration of 1 mg/mL at pH 5 (CHI – M_w = 236.8 kDa, 80% degree of deacetylation (DD) and ALG – M_w = 538 kDa). With these four steps, a CHI/ALG or CHI/ALG-RGD bilayer was formed and this process was repeated 6 times, thus leading to a 6 CHI/ALG or CJI/ALG-RGD bilayered film. The LbL assembly process was performed at room temperature. In the end of the deposition cycles, *i.e.* after the deposition of the 6 bilayers, the ALG structures coated by the $(CHI/ALG)_6$ or $(CHI/ALG\text{-}RGD)_6$ films were stored in deionized water to prevent them from drying and collapsing.

The structures containing the CHI/ALG or CHI/ALG-RGD multilayered films were further cross-linked with a natural-origin, water-soluble cross-linking agent extracted from the fruits of *gardenia jasminoides*, namely genipin (Wako chemical, USA, M_w = 226.23 kDa). A genipin solution (1 mg/mL) was prepared by dissolving the adequate amount of genipin in a water (pH 5)/DMSO mixture at a 4:1 (v/v) ratio. The genipin crosslinking agent solution was incubated with the structures overnight. Afterwards, the structures were extensively washed with ethanol to dissolve the genipin that did not react, followed by air drying.

2.5.3. Zeta (ζ)-potential measurements

Prior to the preparation of the marine polysaccharide-based multilayers, the electrophoretic mobility of the individual CHI, ALG and ALG-RGD aqueous solutions (0.5 mg/mL at pH

5) were investigated by zeta (ζ)-potential measurements, to assess their possible interaction *via* attractive electrostatic interactions. The ζ-potential values of all polymeric aqueous solutions were measured at 25 ºC based on the electrophoretic mobility under an electric field using a Zetasizer Nano-ZS (Malvern Instruments Ltd., Royston, Hertfordshire, UK). The electrophoretic mobility (u) was then converted into a zeta (ζ)-potential value using the Smoluchowski relation ($\zeta = u\eta/\varepsilon$, where η and ε are the viscosity and permittivity of the solution, respectively)[13] Six measurements were performed and averaged for each sample.

2.5.4. Statistical Analysis

Statistical analysis of the data was done using GraphPad 8.3.0.

2.6. Glycidyl methacrylate xanthan gum-based hydrogel

To avoid ALG shape's collapsing, after its liquefaction the resulting CHI/ALG or CHI/ALG-RGD membranes were embedded within a glycidyl methacrylate (GMA)-XG hydrogel further crosslinked by UV light irradiation.

2.6.1. Synthesis of XG-GMA

Chemically modifying natural-based polymers is a common practice in the field of tissue engineering aiming to enhance the cellular behavior. Altering the compounds in order to acquire the ability to photocrosslink is widely used with polymers which intended use is to construct a 3D structure. Such can be attained by the introduction of methacrylic pendant groups into the backbone of natural-based polymers, such as in the of XG. The chemically altered polymers undergo free radical polymerization when under UV light and mixed with a photo-initiator.[14, 15]

In this work, photo-responsive XG hydrogels were prepared as described by Huang and co-workers.[16] The synthetic route is depicted in the Figure 3.5.

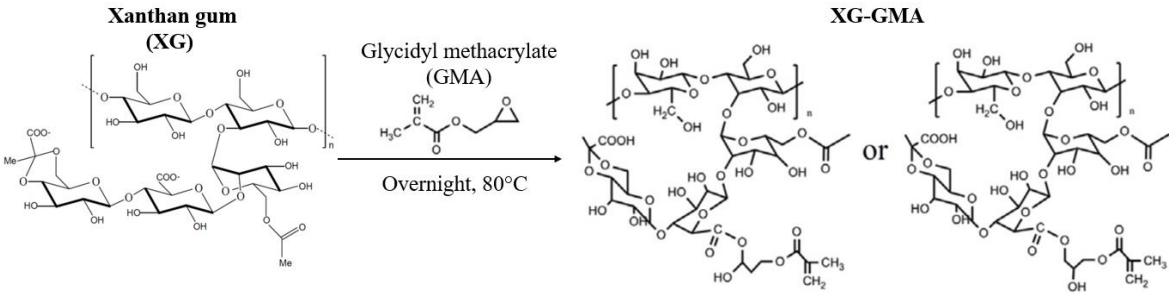

Figure 3.5 – Schematic representation of the covalent chemical synthesis of XG-GMA. Image adapted from [11, 16].

Firstly, a 0.1% (w/v) XG aqueous solution was prepared by dissolving XG powder in deionized water, followed by stirring overnight. Secondly, 100 mL of this solutions was poured into a round-bottom flask and heated to 80°C. Then, 5 mL of GMA (>95%, stabilized with hydroquinone monomethyl ether (MEHQ) from TCI Chemicals) was added to the heated XG solution. After 12-18 h of reaction at 80°C, the resultant solution was collected and dialyzed (M_w cut-off: 12-14 kDa) for 3 days to remove unreacted molecules. Finally, the solution was lyophilized in a freeze-dryer (Telstar LyoQuest Plus Eco, VWR) and stored at 4 °C.

2.6.2. Synthesis of XG-GMA hydrogels

XG-GMA was dissolved in a PBS solution at pH 7.4 containing 0.5% (w/v) 2-hydroxy-4'-(2-hydroxyethoxy)-2-methylpropiophenone (Irgacure, I2959) to achieve a concentration of 0.5% (w/v). This XG-GMA solution was poured into a silicone well and an ALG filament, either with or without the $(CHI/ALG)_6$ or $(CHI/ALG\text{-}RGD)_6$ multilayered film, was immersed on it, leaving both ends of the filament outside the XG-GMA solution in opposing ends (Figure 3.6). Then, the XG-GMA was exposed to UV light irradiation for 60 s (350-420 nm, 200 mW/cm^2), leading to the formation of a photo-crosslinked hydrogel. The resulting hydrogel construct was immersed in a 10 mM EDTA aqueous solution at pH 8 overnight in order to liquify the alginate filament, thus leading to the $(CHI/ALG)_6$ or $(CHI/ALG\text{-}RGD)_6$ free-standing multilayered membrane.

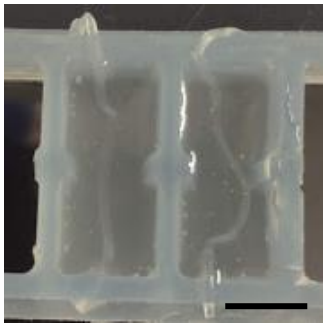

Figure 3.7 – Alginate printed filament, with a $(CHI\text{-}ALG)_6$ multilayered film encapsulated within a XG-GMA aqueous solution prior to UV-light exposure to obtain a robust hydrogel. Scale bar: 5 mm.

2.6.3. Rheological Characterization of XG-GMA

To evaluate the viscosity of the developed XG-GMA hydrogels at 0.5% (w/v), rheological measurements were performed using a Kinexus Ultra+ rheometer (Malvern), fitted with a smooth plate geometry. Briefly, the samples were poured on the rheometer's plate and the chosen test geometry was lowered. The UV light was turned on 20 s after the begin of the test and, then, turned off 3 min later. Control experiments were performed with solely PBS and 0.5% Irgacure. The experiments were performed at room temperature and the samples were stabilized for 5 min before starting the measurements.

2.7. Cell Isolation, Culture and Passaging

The cells used in this thesis were obtained from human umbilical cord provided by the Centro Hospitalar do Baixo Vouga (Aveiro, Portugal) after patient's informed consent and donor anonymization under a strict collaboration protocol established between the University of Aveiro and the Centro Hospitalar do Baixo Vouga, approved by the Human Ethics Committee of the hospital.

2.7.1. Human Umbilical Vein Endothelial Cells

The human umbilical vein endothelial cells (HUVECs) used in this study were obtained by the Centro Hospitalar do Baixo Vouga (Aveiro, Portugal), isolated by the

COMPASS Research Group's researchers, as previously reported by Covas and co-workers,[17] and later stored in a cryotank. Prior to using the cells, a T75 cell culture flask was coated with a 2% gelatin solution (Type B from bovine skin, Sigma Aldrich) and left to incubate for, at least 30 min, at 37.5 °C in a humidified 5% CO_2 atmosphere. This gelatin layer was cleaned with sterile PBS, while the HUVECs were left thawing at room temperature. This cell suspension was seeded into the T75 flask, coated with gelatin, and pre-warmed Medium 199 (M199, Sigma-Aldrich) + 1% GlutaMAX™-I (Thermo Fisher), supplemented with 10% Fetal Bovine Serum (FBS, Alfagene) and 1% Antibiotic-Antimycotic solution (ATB, Thermo Fisher) was added. Medium was changed every 2 to 3 days to assure adequate quantity of nutrients and growth factors to the cells. The cell culture was kept in an incubator at 37.5 °C in a vapor-saturated atmosphere with 5% CO_2.

Upon reaching 80-90% of confluence, the cells were passed to a bigger cell culture flask (T175). This aimed for the removal of the medium from the T75, washing the cells with PBS and add trypsin. The following step was the incubation at 37.5 °C during 5 min. The detachment of the cells was verified using a light microscope (Zeiss, Axiocam 105 color). The reaction was neutralized by using three times the trypsin volume of the same pre-warmed M199 used for cell culture above. To count the cells, it was pipetted 100 µL of the cell suspension to a Neubauer counting chamber (BLAUBRAND), under the light microscope at a 10x magnification. The cell suspension was then centrifuged 5 min at 300 g and the supernatant removed carefully. The remaining pellet was resuspended in M199 and transferred to a T175 already coated with a clean layer of gelatin.

2.7.2. Cell staining

When 80-90% of confluence was achieved, the cells were removed from the T175 cell culture flask and counted. After the removal of the supernatant, the resulting pellet was resuspended in PBS to obtain 1 million of cells per mL. This suspension was protected from the light and 5 µL of Dil Stain (1,1'-Dioctadecyl-3,3,3',3'-Tetramethylindocarbocyanine Perchlorate (DiIC18(3)), Thermo Fisher) was added, as per the fabricator recommendations and incubated for 20 minutes at 37.5°C. The incubated suspension was centrifuged 5 min at 300x *g*, the supernatant removed, and the pellet resuspended in M199 to obtain a final concentration of 40 000 cells per µL.

All HUVECs used were between passages 5 and 7 to ensure the representation of key endothelial characteristics.

2.7.3. Cell seeding

Prior to the seeding of the HUVECs in the microchannels, enclosing or not the $(CHI/ALG)_6$ or $(CHI/ALG\text{-}RGD)_6$ membrane, encapsulated in the hydrogels, the cells were sterilized under UV light for 10-20 min. Then, the hydrogels were submerged in the culture medium (M199 supplemented by 20% fetal bovine serum, and 1% antibiotic) for one to two days at 37.5ºC. The cells were inserted in the channels using a syringe and a needle with an inner diameter of 0.5 mm. The hydrogels with the cells were incubated for 1 day at 37.5°C in a humidified 5% CO_2 atmosphere.

To evaluate the biological performance of the coated channels, *in vitro* cell culture studies were performed.

2.8. Image analysis

The images obtained from the fluorescence microscope were analyzed using ImageJ software. *Z*-stacks were reconstructed with the *z*-projection function of ZEN lite software (Zeizz, Germany), which projects multiple images on a single plane. Following the projections, the channels were merged and colored to obtain the final images. The acquisition of *Z*-stacks and the images' reconstruction were performed to improve the quality of the images and reduce the background caused by the thickness of the hydrogels and *z*-axis orientation of the hydrogels' channels.

2.9. DNA assay

DNA content was quantified using the PicoGreen DNA kit (Molecular Probes) following the manufacturer's instructions. Prior to the DNA quantification, the cells were lysed by osmotic and thermal shock and the supernatant was used for the assay. Triplicates were performed for each sample or assay standard. The plates were read on a microplate

reader (BioTek, USA) using 485 and 528 nm as excitation and emission wavelengths, respectively, according to the spectroscopic properties of the dye. The DNA amounts were calculated using a calibration curve.

Statistical analysis was performed by Shapiro Wilk normality test using Graph Pad Prism 8.3.0 for Windows. After, statistical analysis was performed using one-way ANOVA analysis (Graph Pad Prism 8.3.0 for Windows).

3. References

1. Smidsrød, O., & Skjåk-Bræk, G. (1990). Alginate as immobilization matrix for cells. *Trends in Biotechnology*. https://doi.org/10.1016/0167-7799(90)90139-O

2. Freeman, F. E., & Kelly, D. J. (2017). Tuning Alginate Bioink Stifness and Composition for Controlled Growth Factor Delivery and to Spatially Direct MSC Fate within Bioprinted Tissues, *7*(1), 17042. https://doi.org/10.1038/s41598-017-17286-1

3. Lee, K. Y., & Mooney, D. J. (2012). Alginate: Properties and biomedical applications. *Progress in Polymer Science (Oxford)*, *37*(1), 106–126. https://doi.org/10.1016/j.progpolymsci.2011.06.003

4. Gentile, P., Ghione, C., Ferreira, A. M., Crawford, A., & Hatton, P. V. (2017). Alginate-based hydrogels functionalised at the nanoscale using layer-by-layer assembly for potential cartilage repair. *Biomaterials Science*, *5*(9), 1922–1931. https://doi.org/10.1039/c7bm00525c

5. Yang, J. S., Xie, Y. J., & He, W. (2011, February 11). Research progress on chemical modification of alginate: A review. *Carbohydrate Polymers*. https://doi.org/10.1016/j.carbpol.2010.11.048

6. Lee, K. Y., & Mooney, D. J. (2012). Alginate: Properties and biomedical applications. *Progress in Polymer Science (Oxford)*. Elsevier Ltd. https://doi.org/10.1016/j.progpolymsci.2011.06.003

7. Pujana, M. A., Pérez-Álvarez, L., Iturbe, L. C. C., & Katime, I. (2012). Water dispersible pH-responsive chitosan nanogels modified with biocompatible crosslinking-agents. *Polymer*, *53*(15), 3107–3116. https://doi.org/10.1016/j.polymer.2012.05.027

8. Sousa, M. P., Caridade, S. G., & Mano, J. F. (2017). Control of Cell Alignment and Morphology by Redesigning ECM-Mimetic Nanotopography on Multilayer Membranes. *Advanced Healthcare Materials*, *6*(15). https://doi.org/10.1002/adhm.201601462

9. Wang, J. J., Zeng, Z. W., Xiao, R. Z., Xie, T., Zhou, G. L., Zhan, X. R., & Wang, S. L. (2011). Recent advances of chitosan nanoparticles as drug carriers. *International journal of*

nanomedicine, *6*, 765–74. https://doi.org/10.2147/IJN.S17296

10. Kumar, A., Rao, K. M., & Han, S. S. (2018). Application of xanthan gum as polysaccharide in tissue engineering: A review. *Carbohydrate Polymers*, *180*, 128–144. https://doi.org/10.1016/J.CARBPOL.2017.10.009

11. Petri, D. F. S. (2015). Xanthan gum: A versatile biopolymer for biomedical and technological applications. *Journal of Applied Polymer Science*, *132*(23), n/a-n/a. https://doi.org/10.1002/app.42035

12. Hamman, J. H. (2010). Chitosan Based Polyelectrolyte Complexes as Potential Carrier Materials in Drug Delivery Systems. *Marine Drugs*, *8*(4), 1305–1322. https://doi.org/10.3390/md8041305

13. Hunter, R. J. (2013). *Zeta potential in colloid science: principles and applications* (Vol. 2). Academic press.

14. Pereira, R. F., & Bártolo, P. J. (2015, March 1). 3D Photo-Fabrication for Tissue Engineering and Drug Delivery. *Engineering*. Elsevier Ltd. https://doi.org/10.15302/J-ENG-2015015

15. Babo, P. S., Pires, R. L., Santos, L., Franco, A., Rodrigues, F., Leonor, I., … Gomes, M. E. (2017). Platelet Lysate-Loaded Photocrosslinkable Hyaluronic Acid Hydrogels for Periodontal Endogenous Regenerative Technology. *ACS Biomaterials Science & Engineering*, *3*(7), 1359–1369. https://doi.org/10.1021/acsbiomaterials.6b00508

16. Huang, J., Li, Z., Hu, Q., Chen, G., Ren, Y., Wu, X., & Ren, J. (2018). Bioinspired Anti-digestive Hydrogels Selected by a Simulated Gut Microfluidic Chip for Closing Gastrointestinal Fistula. *iScience*, *8*, 40–48. https://doi.org/10.1016/J.ISCI.2018.09.011

17. Covas, D. T., Siufi, J. L. C., Silva, A. R. L., & Orellana, M. D. (2003). Isolation and culture of umbilical vein mesenchymal stem cells. *Brazilian Journal of Medical and Biological Research*, *36*(9), 1179–1183. https://doi.org/10.1590/S0100-879X2003000900006

Chapter 4 – Embedding layer-by-layer membranes in hydrogels for engineering modular tissue-like constructs

Chapter 4 – Embedding layer-by-layer membranes in hydrogels for engineering modular tissue-like constructs

Catarina A. M. Saraiva, João Borges, João F. Mano

Department of Chemistry, CICECO – Aveiro Institute of Materials, University of Aveiro, Campus Universitário de Santiago, 3810-193 Aveiro, Portugal

Abstract

The presence of a functional vascular network is critical to the long-term viability of larger engineered tissues. Seeing as the engineered structures' core has a short-term cellular viability dueto the structures size being larger than the general diffusion limit for tissues. This hurdle has gathered a lot of attention with several proposals for prevascularization *in vitro*. However, none of them have been entirely successful in attaining a fully functional vascular network. In this work, we propose combining the layer-by-layer (LbL) assembly technology with three dimensional hydrogels. Two combinations of biopolymers were chosen to fabricate the multilayer films, namely CHI/ALG and CHI/ALG-RGD, on top of ALG printed structures. They were then embedded within a xanthan gum solution, having xanthan gum chemically modified with glycidyl methacrylate to be photo-responsive. After the crosslinking of the xanthan gum polymeric chains under UV light irradiation, the hydrogels were submerged in an EDTA aqueous solution to liquify the printed and embedded alginate structure and obtain a hollow channel encompassing the multilayered membranes. Then, human umbilical vein endothelial cells (HUVECs) were cultured in the CHI/ALG and CHI/ALG-RGD-based microchannels for 24 hours, reveling a high cell adhesion on those coated with the $(CHI/ALG\text{-}RGD)_6$ multilayered membrane.

Keywords: chitosan, alginate, 3D bioprinting, layer-by-layer membrane, capillary-like structures, xanthan gum hydrogels, endothelial cells, tissue engineering

1. Introduction

The ability to engineer functional tissue constructs at the micro/nanoscale through the combination of biomaterials, signaling molecules and cells has been one of the key aims of the tissue engineering and regenerative medicine field.[1] Both the use of the Layer-by-

Layer (LbL) multilayered films, made of materials such as, polyelectrolytes, biomolecules, colloid or particles, and hydrogels have provided the scientific community with several breakthroughs.[2–5] However, the idea of combining both is still relatively recent. To date, the prevascularization of tissue engineered constructs has been addressed in two different manners.[2, 6–9] The production of thin membranes using the LbL assembly technology has been oriented to the biomimicy of the native vascular network environment and cellular spatial control during development and differentiation.[2, 8–10] The manufacture of biomaterial-based hydrogels constructs aims to emulate the three-dimensional (3D) representation of the vascular environment by controlling the scaffold design up until the seeding of the cells over the two-dimensional (2D) commonly obtained with LbL.[11–13]

Three decades ago, Decher and co-workers introduced the LbL assembly technology as a simple, inexpensive and highly versatile bottom-up approach to fabricate electrostatically-driven polyelectrolyte multilayered films with precisely tailored properties and functions by resorting to polycations and polyanions assembled in an alternate fashion.[8, 14] Since then, the LbL assembly technology has shown all its versatility in terms of the building blocks that can be assembled into multilayered films. Besides electrostatics, a multitude on non-electrostatic intermolecular interactions also play a key role on the fabrication of highly hydrated multilayered assemblies. Those non-electrostatic based driving forces include hydrogen bonding, hydrophobic and host-guest interactions, coordination chemistry, biological specific interactions, among others.[3, 15–18] The only requisite is that the assembled materials show complementary intermolecular interactions.[18] This means that a vast array of building blocks can be used in the assembled films. Moreover, an important feature of this technology relies on the fabrication of multilayered films under very mild conditions, which means that there is no need for harmful organic solvents, high temperatures, or extreme pH, thus being advantageous for biomedical and biotechnological applications Moreover, virtually any substrate, being planar or more convoluted substrates (*e.g.*, porous, colloidal particles, and cylindrical/tubular structures) of almost any surface chemistry (regardless of size and shape) can be used to fabricate such multilayered films by resorting to different assembly methodologies (*e.g.*, dip-coating, spin-coating, spraying).[15, 19–23]

The most common assembly method is dip-coating, which encompasses multiple cycles of dipping the substrate into aqueous solutions of complementary materials with

intermediate washing/rinsing steps to remove weakly adsorbed layers and avoid the cross-contamination of the materials' solutions.[9] By controlling the number of repetitions of these steps/cycles, i.e. the number of adsorbed layers, one is able to precisely control the thickness of the resulting multilayers.[9, 24, 25] The fabrication of hollow cylindrical/tubular membranes is one of the many structures that this technology enables to attain.[3] The employment of multilayered membranes in the biomedical field is not a new concept with already several examples ranging from the production of biomimetic coatings to the ability of controlling the drug release and cellular adhesion.[15, 17, 26]

The use of hydrogels in tissue engineering came across as a solution to achieve 3D tissue constructs, which can be cell-seeded or cell-laden. Scaffolds encapsulating or entrapping cells within their structure are cell-laden scaffolds, which differ from the cell-seeded ones, where cells are placed on the scaffold and adhere to the surface of the scaffold.[27–29] Nowadays, the use of hydrogels is centered in additive manufacturing of sacrificial and permanent scaffolds.[30–33] Specifically, bioprinted hydrogels have been showing great potential for addressing the problematics of prevascularization.[27, 34, 35] Moreover, photo-crosslinkable hydrogel constructs have been shown to be very attractive to be used in the embedding of printed sacrificial materials.[34, 36]

The use of bioprinting in the fabrication of 3D constructs fit for prevascularization is still a relatively new concept due to the 3D bioprinting technology only coming about in the last decades.[4, 37, 38] Bioprinting techniques are commonly divided in three major categories: extrusion, laser-assisted and inkjet bioprinting. Inkjet-based technique was the first to incorporate the use of cells, due to the simplicity of the adaptation of a standard office inkjet printer.[30, 39, 40] However, its inability to print larger tissue construct sifted the attention to extrusion-based techniques.[30, 41]

This work's idea consisted in the evaluation of the potential to recreate the vascular microenvironment by constructing a hollow channel, lined with LbL CHI/ALG membrane, within a XG-based hydrogel. To construct the membrane, it was chosen the use of CHI and ALG biopolymers due to their biocompatibility, structural resemblance to glycosaminoglycans and their ample successful use in literature.[3, 42, 43] As a LbL substrate it was used an ALG ink due to its ability to retain the shape during the LbL dipping cycles and simplicity in its elimination. Xanthan gum chemically modified with glycidyl methacrylate has shown to have excellent biocompatibility and 3D structural stability after

UV light exposure.[44]

2. Materials and methods

2.1. Materials

Alginate (ALG, M_w = 538 kDa, viscosity ≈250 cP) was purchased as powder from Sigma-Aldrich as used as received. The chitosan (CHI, M_w = 236.8 kDa, 80% degree of deacetylation (DD), viscosity 200−800 cP) was acquired from Primex EHF (Siglufjordur, Iceland). Xanthan gum (XG) powder was obtained from the commercial store Celeiro (Doves Farm Foods Ltd, distributed by Bricer Unipessoal, Portugal).

2.2. Methods

2.2.1. Preparation of the ink

The preparation of the ink followed the method described by Freeman & Kelly, with minor changes in the viscosity of the ink.[45] Briefly, an ALG ink solution was prepared at 5% (w/v) in phosphate buffer solution (PBS, Sigma Aldrich). Moreover, a 60 mM calcium chloride ($CaCl_2$) aqueous solution was prepared to crosslink the ALG ink. To form the ALG ink, these solutions were pre-crosslinked by mixing the two at a volumetric ratio (v/v) of 25:9 (alginate solution:$CaCl_2$ solution). The inks were left to crosslink for 30 minutes prior to printing.

2.2.2. 3D-Printing using alginate ink

Each designed structure was then sliced into layers depending on the height of the structure. In this case only one layer was needed to be printed to form the 3D structure. A 3D Cellink Inkredible bioprinter (Cellink, Sweden) and a 23G (0.33 mm of inner diameter) needle were used to print the inks.

2.2.3. 3D Modelling using CAD

The overall design of the scaffold consisted on a cylinder with a diameter of 0.33 mm (Figure 3.4a), to match the internal diameter of the needle used. The cylinder's length varied between 1 to 5 cm.

2.2.4. Printing using Repetier-Host

The printing settings used were: extrusion pressure between 45 to 55 kPa and needle speed of 25 mm/s. All the printing was performed at room temperature. The extrusion pressure, which was set on the Repetier-Host 3D printer had to be constantly optimized during the printing process. The printing process started 30 minutes after the mixture of the alginate and $CaCl_2$. Afterwards, the printed structures were immersed in a 60 mM $CaCl_2$ aqueous solution for 5 to 10 minutes to further crosslink the structure.

2.2.5. Production of chitosan-alginate multilayered films

2.2.5.1. Quartz crystal microbalance with dissipation monitoring

The build-up of the CHI/ALG and the CHI/ALG-RGD was monitored in situ by quartz crystal microbalance (QCM-D, Q-Sense Pro, Biolin Scientific, Sweden) in a liquid environment. The gold-coated quartz crystal substrates were excited at multiple overtones (1, 3, 5, 7, 9, and 11, corresponding to 5, 15, 25, 35, 45, and 55 MHz, respectively). Before the testing on the CHI and ALGs solutions, the crystals were thoroughly cleaned. the Au-plated quartz crystals were alternately exposed to 0.5 mg/mL CHI (6 min adsorption time) and ALG (6 min adsorption time) or ALG-RGD (6 min adsorption time) aqueous solutions at pH 5, rendering the surface positively and negatively charged respectively, to build-up $(CHI/ALG)_6$ and $(CHI/ALG\text{-}RGD)_6$ multilayered films. After each deposition step, the substrates were rinsed with an aqueous solution at pH 5 for 4 min to remove weakly adsorbed molecules. The final multilayered thin films were dried under a soft stream of N_2.

2.2.5.2. Multilayered membranes build-up

The build-up of the CHI/ALG multilayered films on the ALG-based cylindrical printed structures was performed using an automatic home-made dipping robot (CORPUS®). Briefly, the structures were alternately dipped in the aqueous solutions of the CHI and ALG biopolymers at pH 5 for 6 min each. In-between the immersion of the structures in the CHI and ALG aqueous solutions, the structures were dipped in washing steps (4 min each) at room temperature. The polyelectrolyte solutions were prepared at a concentration of 1 mg/mL at pH 5(CHI – M_w = 236,8 kDa, 80% degree of deacetylation, viscosity 200−800 cP and ALG – M_w = 538 kDa, viscosity ≈250 cP). With these four steps a CHI/ALG bilayer was formed and this process was repeated 6 times, thus leading to a CHI/ALG membrane with six bilayers.

A genipin (Wako chemical, USA) solution (1 mg/mL) was prepared by dissolving the adequate amount of genipin in the same solution as the washing buffer previously prepared for the LbL process at pH 5/DMSO mixture at a 4:1 (v/v) ratio). The genipin crosslinking agent solution was incubated with the cylindrical structures overnight. Afterwards, the structures were extensively washed with ethanol.

2.2.6. Zeta potential

Electrophoretic mobility measurements were performed with a Zetasizer Nano Series (Malvern Instruments). The samples measured were CHI 0.5 mg/mL, ALG 0.5 mg/mL and ALG-RGD 0.5 mg/mL aqueous solutions at pH 5.

2.2.7. Glycidyl methacrylate xanthan gum-based hydrogel

2.2.7.1. Synthesis of XG-GMA

To achieve photo responsive xanthan gum hydrogel it was followed the procedure reported by Huang and co-worker.[44] Firstly, a 0.1% (w/v) XG aqueous solution was prepared by dissolving XG powder in deionized water, followed by stirring overnight. Secondly, 100 mL of this solutions was poured into a round-bottom flask and heated to 80°C. Then, 5 mL of GMA (>95%, stabilized with hydroquinone monomethyl ether (MEHQ) from TCI Chemicals). After 12-18 h of reaction at 80°C, the resultant solution was collected and

dialyzed for 3 days, using dialysis membranes (M_w cut-off: 12-14 kDa) to remove unreacted GMA residues. Finally, the solution was lyophilized in a freeze-dryer (Telstar LyoQuest Plus Eco, VWR) and stored at 4 °C.

2.2.7.2. Synthesis of XG-GMA hydrogels

XG-MA was dissolved in a PBS solution at pH 7.4 containing 0.5% (w/v) 2-hydroxy-4'-(2-hydroxyethoxy)-2-methylpropiophenone (Irgacure, I2959) to achieve a concentration of 0.5% (w/v). This XG-GMA solution was poured into a silicone well and an ALG filament, either with or without the CHI/ALG multilayered membrane, was immersed in the hydrogel, leaving both ends of the filament outside the hydrogel in opposing ends. Next, the hydrogels were exposed to UV light irradiation for 60 s (350-420 nm, 200 mW/cm^2), forming a photo-crosslinked hydrogel. The hydrogel was immersed in an EDTA solution (10 mM) overnight in order to liquify the alginate filament, thus leading to the CHI/ALG multilayered membrane.

2.2.8. Cell seeding

Prior to the seeding of the HUVECs in the channels of the hydrogels, they were sterilized under UV light for 10 to 20 minutes. Some of the membranes were injected with fibronectin and left to incubate overnight. The channels were then washed with M199 to remove the remaining fibronectin. The hydrogels were submerged in the culture medium (M199 supplemented by 20% fetal bovine serum, and 1% antibiotic) for one to two days at 37.5ºC. The cells were inserted in the channels using a syringe and a needle with an inner diameter of 0.5 mm. The hydrogels with the cells were incubated for 1 day at 37.5°C in a humidified 5% CO_2 atmosphere.

2.2.9. Cellular viability assay

To evaluate cell viability was assessed after 24 hours of incubation using the live/dead assay (calcein AM/propidium iodide (PI) staining). Briefly, the hydrogels were incubated for 20 min with 2 µL calcein AM (1 mg mL^{-1}, Molecular Probes, Invitrogen, USA) and 1 µL PI (1 mg mL^{-1}, Molecular Probes, Invitrogen, USA) in 1 mL PBS protected from

light. The channels were washed with PBS to remove residual fluorescent and immediately imaged in an upright widefield microscope (Axio imager M2, Carl Zeiss, Germany). The images were acquired at the wavelengths of 520/525 nm and 607/650 nm for the excitation of calcein and propidium iodide, respectively. To evaluate the adhesion of the cells to the membranes, membrane-free hydrogels where used.

2.2.10. DNA assay

DNA content was quantified using the PicoGreen DNA kit (Molecular Probes) according to the instructions from the manufacturer. Prior to DNA quantification, cells were lysed by osmotic and thermal shock and the supernatant was used for the assay. Triplicates were performed for each sample or assay standard. The plates were read on a microplate reader (BioTek, USA) using 485 and 528 nm as excitation and emission wavelengths, respectively, according to the spectroscopic properties of the dye. The DNA amounts were calculated using a calibration curve.

3. Results and discussion

In this work, we aim to embed a multilayered membrane in a hydrogel in order to obtain a within the hydrogel hollow channel coated with the multilayered membrane were cells could be cultured (Figure 4.1). The materials proposed for the multilayered membrane would be chitosan and alginate, two biopolymers biocompatible and with a variety of literacy denoting their successful use with the layer-by-layer assembly method. This membrane would be built upon structures printed using an alginate ink. To embed these, it would be xanthan gum hydrogel, seeing as it is also biocompatible. To culture inside these channels it was chosen human umbilical vein endothelial cells (HUVECs).

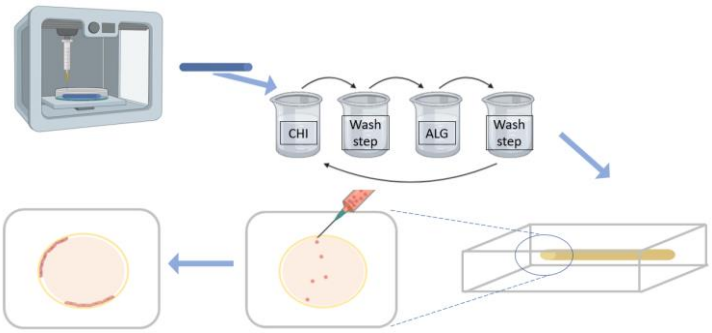

Figure 4.8 – Schematic representation of the steps to obtain a $(CHI/ALG)_6$ or $(CHI/ALG\text{-}RGD)_6$ multilayered membrane embedded in a XG-based hydrogel for cell culture.

3.1. Printing

The shapes chosen to be printed had the goal to demonstrate nor only the versatility of the printing techniques in printing different geometries in a personalized fashion but also their ability to be perfused when within a hydrogel (Figure 4.2). The possibility of having more complex shapes than a straight line, which can be also perfused, opens new avenues in other designs that not only vary widely within the 2D dimensions (*x* and *y* axes) but also in the z axis.

The alginate ink proposed by Freeman and Kelly[45] was not compatible with the Cellink Inkredible bioprinter available at our lab. The lowest printing speed of the bioprinter was too fast and the ink was extruded to the petri dish in a drop-by-drop manner. By rising the alginate concentration to 5% (w/v), the solution extruded from the cartridge was viscous enough to be a continuous line.

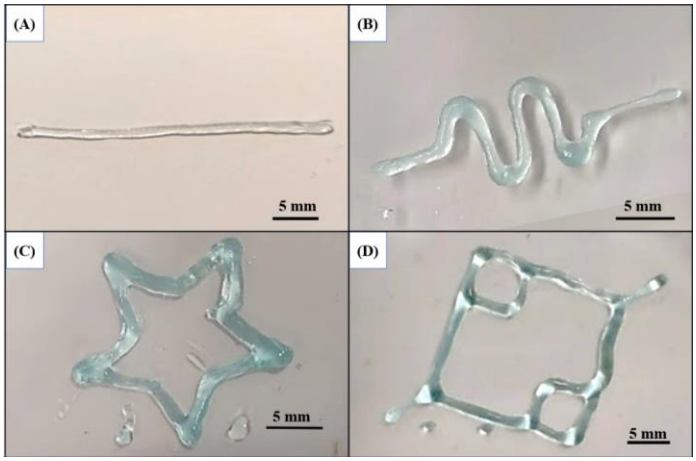

Figure 4.9 – Photograph of the printed alginate structures after the $CaCl_2$ crosslinking bath. (A) cylinder; (B)

sinusoidal; (C) star; (D) capillary representations. Scale bars, 5mm.

The obtained structures have an inner diameter due to the natural spreading of the ink as it exits the needle. The choice of dissolving the alginate in PBS contributed to reduce the spreading ratio of the alginate ink. The influence of phosphate ion in the alginate inks' mechanical properties has been previously demonstrated.[45, 46] The constructs printed were structurally strong enough to be picked up from the petri dish and still maintain their shape with minimal deformation due to its own weight, as shown in Figure 4.3.

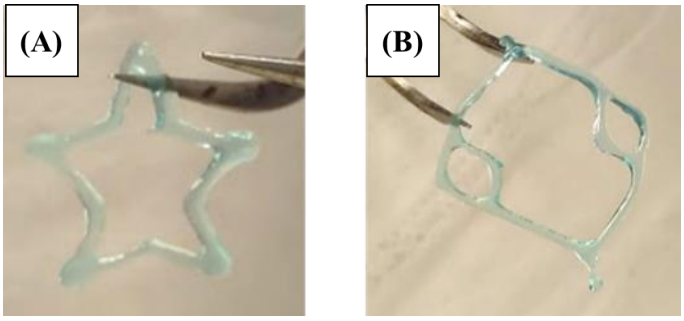

Figure 4.3 – Printed designs held up by a tweezer.

3.2. Preparation and physicochemical and morphological characterization of chitosan-alginate multilayered films

3.2.1. Electrostatic-driven Layer-by-Layer assembly of multilayered films

LbL films encompassing positively charged chitosan and oppositely charged alginate were adsorbed on the personalized printed constructs. CHI and ALG were chosen as the biopolymers to build-up the multilayered films due to their intrinsic features, including biocompatibility, biodegradability, bioavailability (biopolymers widely available in the sea), and non-immunogenic properties, being very appealing for biotechnological and biomedical applications. Moreover, the presence of cationic (protonated amine groups) and anionic (deprotonated carboxyl groups) functional groups in CHI and ALG structures at certain pH conditions will be key to trigger the assembly of the biopolymers into electrostatically-driven LbL films.

3.2.2. Zeta (ζ)-Potential Measurements

The positive and negative electrical charges assigned to CHI and ALG, respectively, is dependent on the dissociation constant (pK_a) of the biopolymers and pH of the working solutions. As such, the electrical charge of freshly prepared CHI and ALG aqueous solutions at pH 5 (working pH) was assessed by ζ-potential measurements in order to determine the possible interaction and successful build-up of multilayered films encompassing both biopolymers. The freshly prepared CHI, ALG and ALG-RDG aqueous solutions (0.5 mg/mL at pH 5) exhibited ζ-potentials of +17.9 ± 0.4 mV, −23.4 ± 1.6 mV and −19.7 ± 2.7 mV (Table 4.1), thus confirming the cationic nature of the CHI and anionic nature of the ALG and ALG-RGD biopolymer solutions, respectively, at pH 5. Based on the gathered values, we hypothesize that the positively charged CHI and the negatively charged ALG molecules could be used to build-up electrostatic based multilayered assemblies.

Table 4.1– Mean ζ-potential and respective standard deviation of CHI, ALG, and ALG-RGD 0.5 mg/mL aqueous solutions at pH 5.

Solutions	Mean ζ-potential (mV)	Standard deviation
ALG	-23.4	1.6
ALG-RGD	-19.7	2.7
CHI	+17.9	0.4

3.2.3. Build-up and characterization of CHI/ALG multilayered films

The possible step-by-step build-up of a six CHI/ALG and six CHI/ALG-RGD bilayer films on a gold-plated quartz crystal surface, by employing the electrostatic-driven LbL assembly interaction between oppositely charged materials, was assessed using the QCM-D apparatus. This technique is more than a mass sensing device allowing us to obtain information on the mass changes per adsorbed layer, though the change in the frequency shift ($\Delta f_n/n$) of the gold-coated quartz crystal substrate, as well as on the viscoelasticity of

the adsorbed layers, making use of the energy dissipation in the mechanical oscillation of the gold-coated quartz crystal substrate.

Figure 4.4 shows the normalized frequency shift ($\Delta f_n/n$) and the dissipation factor (ΔD_{nn}) obtained at the 3rd (*n = 3*; 15 MHz), 5th (*n = 5*; 25 MHz), 7th (*n = 7*; 35 MHz), 9th overtones (*n = 9*; 45 MHz) and 11th overtones (*n = 11*; 55 MHz) during the build-up of six bilayers of CHI/ALG (Figure 4.3A) and CHI/ALG-RGD (Figure 4.3B) films onto the gold-coated quartz crystal substrate.

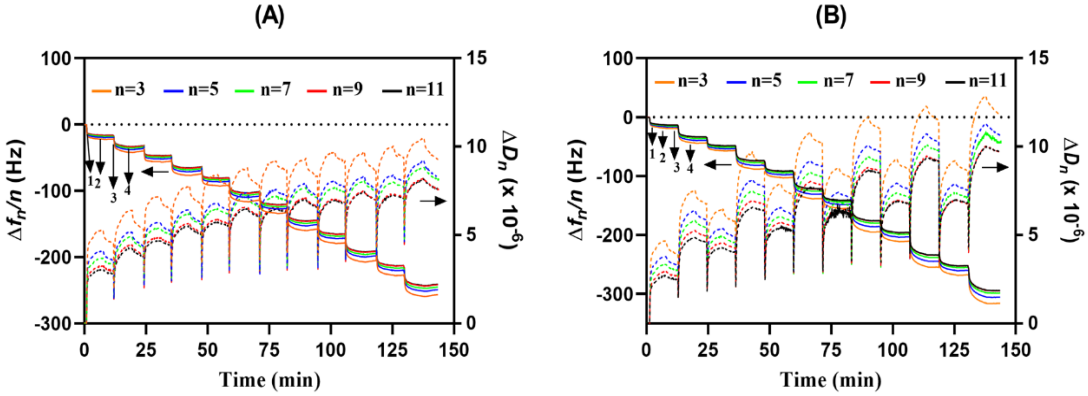

Figure 4.4 – QCM-D monitoring of the normalized frequency ($\Delta f_n/n$) and dissipation (ΔD_n) shifts as a function of time for the LbL deposition of $(CHI/ALG)_6$ **(A)** and $(CHI/ALG\text{-}RGD)_6$ **(B)** onto gold-coated quartz crystal sensors and intermediate rinsing steps. Numbers refer to the adsorption of CHI (1), ALG or ALG-RGD (3), and rinsing steps (2 and 4).

The successive decrease in the $\Delta f_n/n$ and ΔD_n as a function of time after the injection of each material (CHI, ALG or ALG-RGD at 0.5 mg/mL at pH 5) onto the quartz substrate not only confirms the deposition of each material and, thus, increase in the adsorbed mass at every stage of the adsorption process, but also indicates a gradual and stable growth of the multilayered films at the nanoscale. Moreover, the continuous increase in the ΔD_n reveals the viscoelastic behavior of the adsorbed layers, meaning that the multilayered film is not rigid and shows damping properties, which is a typical behavior of polymeric systems. [17, 47] With the increase in the energy dissipation values after each deposition step, the overtones became more separated, which is a characteristic behavior of a soft and hydrated film, and suggests that the viscoelastic properties of the adsorbed films are not constant throughout the assembly process. The sequential decrease of the frequency shift together with the increase of the energy dissipation implies that at the working pH of 5 the negatively charged ALG molecule adsorbed onto the positively charged CHI layer. Such behavior confirms the

effective interaction between the two molecules and the successful and stable build-up of multilayered films.

A more pronounced decrease in the $\Delta f_n/n$, as well as increase in the ΔD_n was denoted for the $(CHI/ALG\text{-}RGD)_6$ film, which is assigned to the functionalization of the ALG biopolymer with the RDG sequence that provides additional sites for the interaction with the CHI biopolymer. As such a higher adsorbed mass and viscoelasticity was observed in the case of the $(CHI/ALG\text{-}RGD)_6$ multilayered film. In both multilayered films, the washing steps led to negligible changes in the $\Delta f_7/7$ and ΔD_7 values, suggesting the strong association of both materials and the irreversible nature of the adsorption process. In overall, the QCM-D results confirm that both the $(CHI/ALG)_6$ and the $(CHI/ALG\text{-}RGD)_6$ multilayered films were successfully conceived by exploring the attractive electrostatic interactions between oppositely charged building blocks.

Then, the same LbL assembly process was performed on the bioprinted ALG structure using an automated dipping robot and 1 mg/mL CHI, ALG or ALG-RGD aqueous solutions at pH 5. In order to assess the formation of the $(CHI/ALG)_6$ multilayered membrane on the ALG structure's surface by fluorescence microscopy, the CHI biopolymer was labelled with rhodamine B isothiocyanate (RITC). As shown in the Figure 4.5, the $(CHI\text{-}RITC/ALG)_6$ film was deposited on the ALG printed structure.

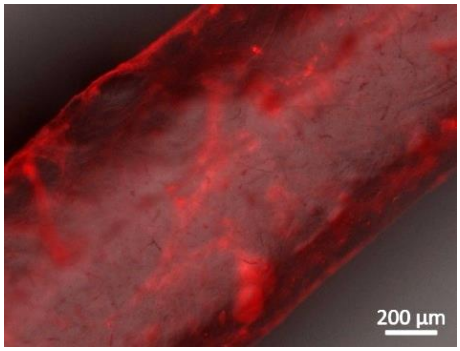

Figure 4.5 – Rrepresentative fluorescence microscopy image of the ($RITC$-labeled $CHI/ALG)_6$ multilayered film deposited onto the ALG printed structure. Scale bar: 200 µm.

3.3. Glycidyl methacrylate xanthan gum hydrogel

The XG-GMA aqueous solution obtained after dissolving XG-GMA in PBS at pH 7.4, with 0.5% (w/v) Irgacure, at a concentration of 0.5% (w/v), was poured into the silicone

molds and reticulated under UV light. It was possible to assess by naked eye that the photo-crosslinking of the solution was successful when the hydrogel was removed from the mold (Figure 4.6), due to the ability of the hydrogel to retain the mold's shape.

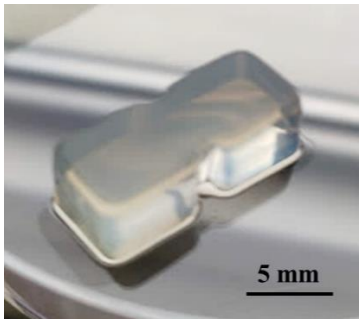

Figure 4.6 – XG-GMA hydrogel (without inner channel) after being removed from the silicone mold. Scale bar: 5 mm.

For the hydrogels incorporating the ALG printed structure with or without the $(CHI/ALG)_6$ multilayered film, the structure was placed in the center of the XG-GMA aqueous solution in the mold before being exposed to the UV light for 60 s. Then, the ALG printed structure, with or without the $(CHI/ALG)_6$ multilayered membrane, was liquified with an EDTA aqueous solution at pH 8, thus resulting in a perfusable microchannel within the XG-GMA hydrogel that held the shape of the printed ALG structure. In order to verify the perfusion extension of the channel created within the hydrogel, a fluorescent dye aqueous solution was injected into the microchannel. The naked-eye visible movement of the fluorescent dye solution through the microchannel across the hydrogel proved the success of the liquefaction of the printed ALG structure (Figure 4.7).

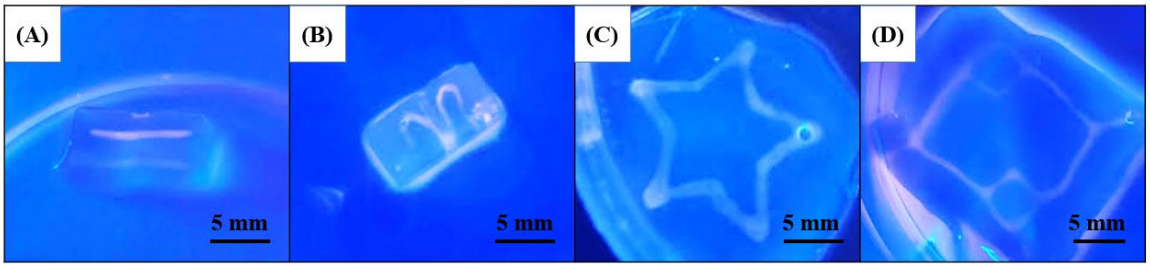

Figure 4.7 – Orange fluorescent solution injected into the channel obtained by the liquification of the alginate printed structure viewed under UV light. (A) cylinder; (B) sinusoidal; (C) star; (D) capillary representations. Scale bars: 5 mm.

3.3.1. Rheological characterization of the XG-GMA hydrogel

The photo-gelling response of the XG-GMA solution at 0.5% (w/v) with the photo-initiator used in this work was characterized under UV light exposure. Figure 4.8 shows the characterization of the XG-GMA hydrogel's sample shift from the solution state to the gelled state behavior throughout the time and the frequency spectra and the time sweep, both obtained at room temperature, where the UV light was turned on 20 s after the initiation of the analyze. The sudden and sharp rise of both moduli *G'* (elastic modulus) and *G''* (viscous modulus) right after the 20 s mark illustrates the beginning of the photo-reticulation of the solution. The change in the elastic modulus' slope after the sharp rise corresponds to the behavior of the gel.

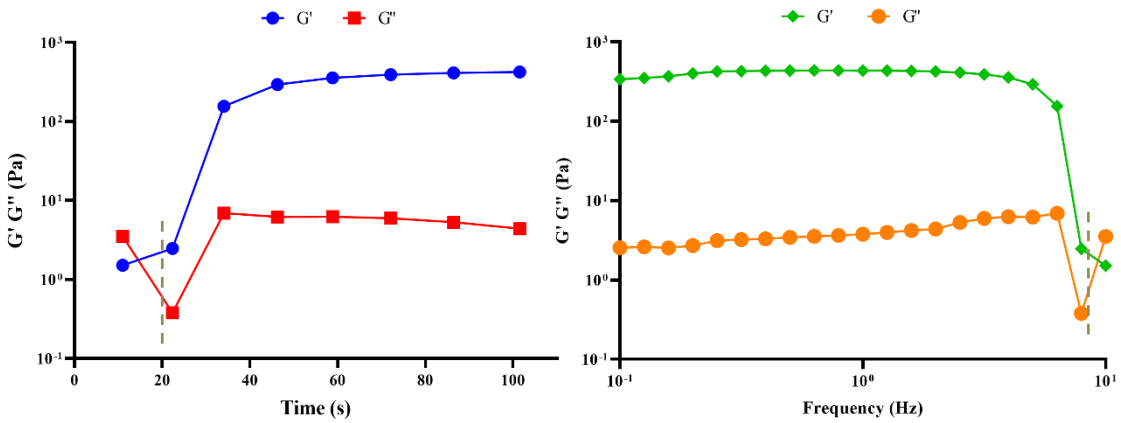

Figure 4.810 – **(A)** Time sweep at 1 Hz of XG-GMA 0.5% (w/v) in Irgacure 0.5% (w/v). **(B)** Frequency spectra of XG-GMA 0.5% (w/v) in Irgacure 0.5% (w/v). The dashed lines shown are drawn to guide the eye to the time point where the UV light was turned on.

3.4. *In vitro* biological performance

3.4.1. Cellular Adhesion and viability

In order to check cell viability, it was performed a calcein/propidium iodide (PI) staining, where viable cells are labeled with green fluorescent dye calcein and the red fluorescent dye PI binds to the DNA of the dead cells.

In general, 24 h after injecting the cells into the channels, it is visible a large difference between dead (red) and viable (green) cells, where the first ones are visibly more

predominate (Figure 4.9). The hydrogels which channels were lined with the membranes with the RGD labeled alginate showed a higher quantity of cells, both viable and non-viable cells, which may be due to the existence of sites for integrins to bind to, provided by the RGD labeled alginate.

In order to assess the cellular adhesion on the $(CHI/ALG\text{-}RGD)_6$ multilayered membrane, some channels were flushed with PBS before the calcein/propidium iodide staining, 24 h after seeding HUVECs stained with Dil. After the medium M199 that surrounds the hydrogels was removed, the DPBS was slowly and carefully injected into the channels to clear out the cells that had not adhered to the channel walls. The hydrogels were then viewed under a fluorescent microscope afterwards incubating for 20 minutes at 37.5°C and 5% CO_2 with the dyes calcein and PI.

It was possible to visualize a clear lower number of cells present in the channels that were flushed with DPBS. Still, the hydrogels with the $(CHI/ALG\text{-}RGD)_6$ membrane and without membrane showed a higher number of cells when compared to the hydrogels with the $(CHI\text{-}ALG)_6$ membrane. Comparing the hydrogels with the $(CHI/ALG\text{-}RGD)_6$ with the ones that do not have a LbL membrane, it was not viewed a considerate difference in the number of cells within the channels.

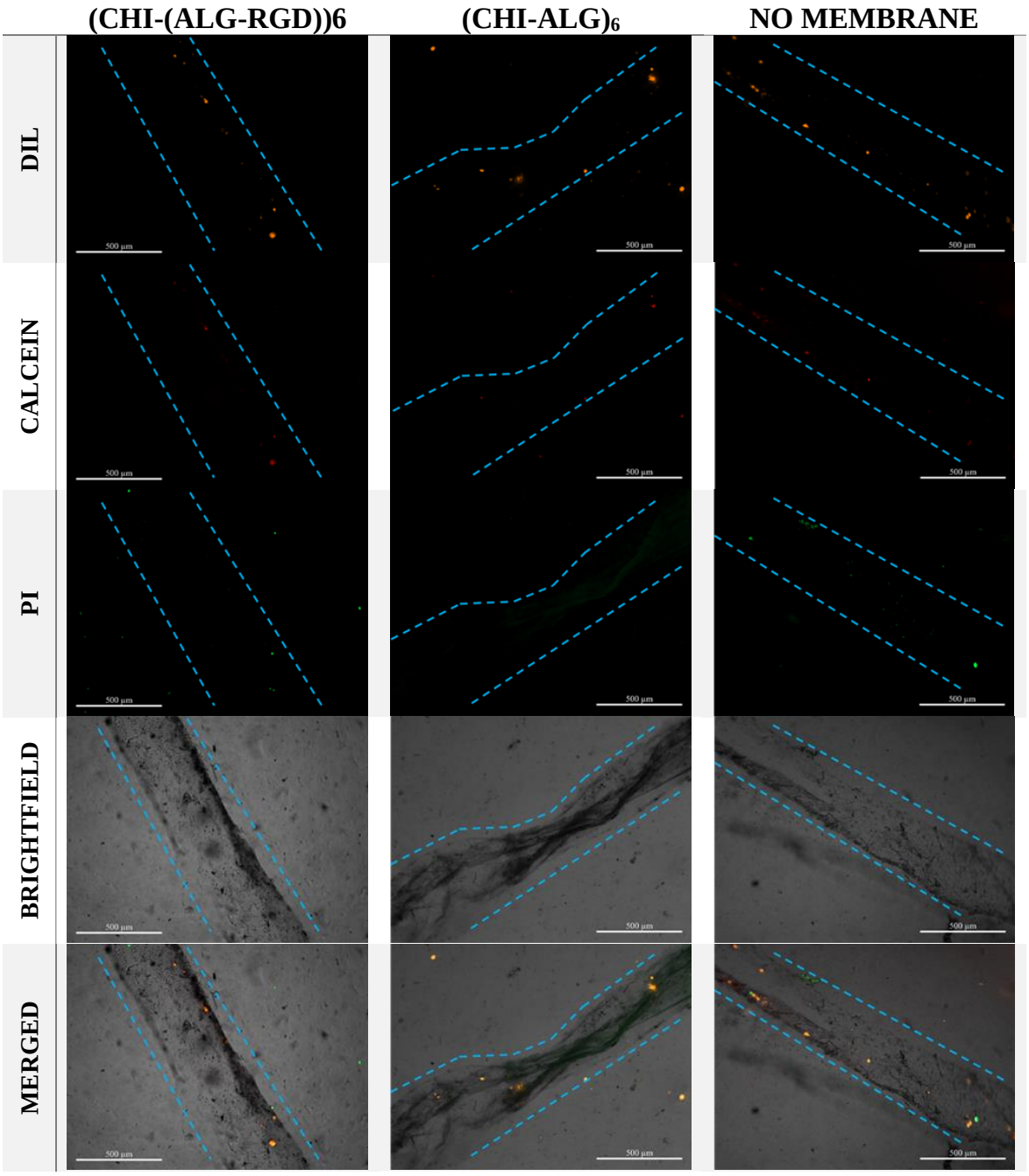

Figure 4.9 – Live/dead assay of HUVECs seeded onto the microchannel-free and microchannel containing the $(CHI/ALG\text{-}RGD)_6$ or $(CHI/ALG)_6$ multilayered membrane embedded in the XG-GMA hydrogels. Micrographs obtained 24 hours after cell seeding. Dashed blue lines were placed to delimitate the channel. Scale bars: 500 µm.

3.4.2. DNA Quantification

Cell adhesion differences were quantified by the evaluation of the DNA present in the samples (Figure 4.10). The results obtained support the information shown in the

fluorescence microscope that, 24 hours after being injected in the cells, the hydrogels with channels lined with a membrane contained a larger amount of cells. Specifically, the hydrogels with membranes which were fabricated using the RGD labeled ALG showed a larger amount of DNA over all. By quantifying the DNA present in the channels we demonstrated the presence of the adhered cells.

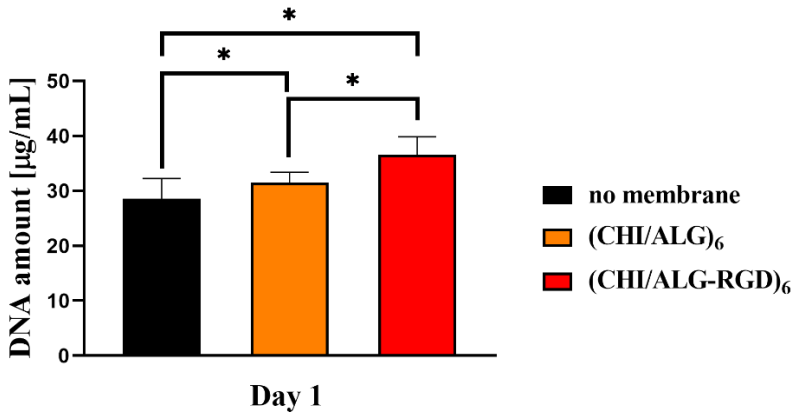

Figure 4.10 – DNA assay on the hydrogels 24 hours after seeding. The HUVECs were seed within the channel without membrane, in channels lined with $(CHI/ALG)_6$ membrane and in channels lined with a $(CHI/ALG\text{-}RGD)_6$. Significant differences between each condition were found for p 0.05(*).

4. Conclusion

In conclusion, we have developed combined structures inspired by the native capillary tissue environment. These structures attempt to recreate the physical microenvironment of the capillary tissues by combining hydrogels and multilayered membranes fabricated with the layer-by-layer technique.

The structures were obtained by embedding membranes composed of six bilayers of marine-origin polymers into a xanthan gum solution that was then reticulated under UV light exposure. Prior to their embedding, these membranes were assembled on top of an alginate printed structure. In the hollow space within the membrane, left behind by the liquification of the alginate printed structure, were cultured HUVECs.

After seeding the cells for 24 h, it was possible to assess a higher cell adhesion to the $(CHI/ALG\text{-}RGD)_6$ multilayered membrane. The results were supported by the quantification of the DNA in each construct, which confirmed the adhesion of the cells. As such, we can conclude that the combination of the hydrogel network and multilayered membranes shows

promise in the engineering of capillary-like structures.

5. References

1. Bittner, S. M., Guo, J. L., Melchiorri, A., & Mikos, A. G. (2018). Three-dimensional printing of multilayered tissue engineering scaffolds. *Materials Today*, *21*(8), 861–874. https://doi.org/10.1016/j.mattod.2018.02.006
2. Zhang, S., Xing, M., & Li, B. (2018). Biomimetic layer-by-layer self-assembly of nanofilms, nanocoatings, and 3D scaffolds for tissue engineering. *International Journal of Molecular Sciences*. MDPI AG. https://doi.org/10.3390/ijms19061641
3. Silva, J. M., Duarte, A. R. C., Custódio, C. A., Sher, P., Neto, A. I., Pinho, A. C. M., Fonseca, J., Reis, R., L. & Mano, J. F. (2014). Nanostructured Hollow Tubes Based on Chitosan and Alginate Multilayers. *Advanced Healthcare Materials*, *3*, 433–440. https://doi.org/10.1002/adhm.201300265
4. Khademhosseini, A., & Langer, R. (2016). A decade of progress in tissue engineering. *Nature Protocols*, *11*(10), 1775–1781. https://doi.org/10.1038/nprot.2016.123
5. Sharma, D., Ross, D., Wang, G., Jia, W., Kirkpatrick, S. J., & Zhao, F. (2019). Upgrading prevascularization in tissue engineering: A review of strategies for promoting highly organized microvascular network formation. *Acta Biomaterialia*. https://doi.org/10.1016/j.actbio.2019.03.016
6. Liew, A. W. L., & Zhang, Y. (2017). In vitro pre-vascularization strategies for tissue engineered constructs-bioprinting and others. *International Journal of Bioprinting*, *3*(1), 3–17. https://doi.org/10.18063/IJB.2017.01.008
7. Dzobo, K., Thomford, N. E., Senthebane, D. A., Shipanga, H., Rowe, A., Dandara, C., Pillay, M., Motaung, K. S., & Motaung, K. S. C. M. (2018). Advances in Regenerative Medicine and Tissue Engineering: Innovation and Transformation of Medicine. *Stem Cells International*, *2018*, 1–24. https://doi.org/10.1155/2018/2495848
8. Tang, Z., Wang, Y., Podsiadlo, P., & Kotov, N. A. (2006, December 18). Biomedical applications of layer-by-layer assembly: From biomimetics to tissue engineering. *Advanced Materials*. https://doi.org/10.1002/adma.200600113
9. Ren, K., Hu, M., Zhang, H., Li, B., Lei, W., Chen, J., Chang, H., Wang, L., & Ji, J. (2019). Layer-by-layer assembly as a robust method to construct extracellular matrix mimic surfaces to modulate cell behavior. *Progress in Polymer Science*. https://doi.org/10.1016/j.progpolymsci.2019.02.004
10. Zhao, S., Caruso, F., Dahne, L., Decher, G., Geest, B. G. De, Fan, J., Feliu, Neus, Gogotsi, Y., Hammond, P. T., Hersam, M. C., Khademhosseini, A., Kotov, N., Leporatti, S., Li, Y.,

Lisdat, F., Liz-Marzan, L. M., Moya, S., Mulvaney, P., Rogach, A. L., Roy, S., Shchukin, D. G., Skirtach, A. G., Stevens, M. M., Sukhorukov, G. B., Weiss, . S., Yue, Z., Zhu, D., & Parak, W. J. (2019). The Future of Layer-by-Layer Assembly: A Tribute to ACS Nano Associate Editor Helmuth Mö hwald. *ACS Nano*, *13*, 6151−6169. https://doi.org/10.1021/acsnano.9b03326

11. Hinton, T. J., Jallerat, Q., Palchesko, R. N., Park, J. H., Grodzicki, M. S., Shue, H. J., Ramadan, M. H., Hudson, A. R., & Feinberg, A. W.(2015). Three-dimensional printing of complex biological structures by freeform reversible embedding of suspended hydrogels. *Science Advances*, *1*(9). https://doi.org/10.1126/sciadv.1500758
12. Kucukgul, C., Ozler, S. B., Inci, I., Karakas, E., Irmak, S., Gozuacik, D., Taralp, A., & Koc, B. (2015). 3D bioprinting of biomimetic aortic vascular constructs with self-supporting cells. *Biotechnology and Bioengineering*, *112*(4), 811–821. https://doi.org/10.1002/bit.25493
13. Huh, D., Hamilton, G. A., & Ingber, D. E. (2011). From 3D cell culture to organs-on-chips. *Trends in Cell Biology*, *21*(12), 745–754. https://doi.org/10.1016/J.TCB.2011.09.005
14. Correia, C. R., Reis, R. L., & Mano, J. F. (2013). Multilayered Hierarchical Capsules Providing Cell Adhesion Sites. *Biomacromolecules*, *14*(3), 743–751. https://doi.org/10.1021/bm301833z
15. Costa, R. R., Custódio, C. A., Arias, F. J., Rodríguez-Cabello, J. C., & Mano, J. F. (2011). Layer-by-Layer Assembly of Chitosan and Recombinant Biopolymers into Biomimetic Coatings with Multiple Stimuli-Responsive Properties. *Small*, *7*(18), 2640–2649. https://doi.org/10.1002/smll.201100875
16. Matsusaki, M., Ajiro, H., Kida, T., Serizawa, T., & Akashi, M. (2012). Layer-by-Layer Assembly Through Weak Interactions and Their Biomedical Applications. *Advanced Materials*, *24*(4), 454–474. https://doi.org/10.1002/adma.201103698
17. Boudou, T., Crouzier, T., Ren, K., Blin, G., & Picart, C. (2010). Multiple Functionalities of Polyelectrolyte Multilayer Films: New Biomedical Applications. *Advanced Materials*, *22*(4), 441–467. https://doi.org/10.1002/adma.200901327
18. Borges, J., & Mano, J. F. (2014). Molecular Interactions Driving the Layer-by-Layer Assembly of Multilayers. *Chemical Reviews*, *114*, 8883–8942. https://doi.org/10.1021/cr400531v
19. Sher, P., Custódio, C. A., & Mano, J. F. (2010). Layer-By-Layer Technique for Producing Porous Nanostructured 3D Constructs Using Moldable Freeform Assembly of Spherical Templates. *Small*, *6*(23), 2644–2648. https://doi.org/10.1002/smll.201001066
20. Björnmalm, M., Thurecht, K. J., Michael, M., Scott, A. M., & Caruso, F. (2017). Bridging Bio–Nano Science and Cancer Nanomedicine. *ACS Nano*, *11*(10), 9594–9613.

https://doi.org/10.1021/acsnano.7b04855

21. Schaaf, P., Voegel, J.-C., Jierry, L., & Boulmedais, F. (2012). Spray-Assisted Polyelectrolyte Multilayer Buildup: from Step-by-Step to Single-Step Polyelectrolyte Film Constructions. *Advanced Materials*, *24*(8), 1001–1016. https://doi.org/10.1002/adma.201104227
22. Piccinini, E., Bliem, C., Reiner-Rozman, C., Battaglini, F., Azzaroni, O., & Knoll, W. (2017). Enzyme-polyelectrolyte multilayer assemblies on reduced graphene oxide field-effect transistors for biosensing applications. *Biosensors and Bioelectronics*, *92*, 661–667. https://doi.org/10.1016/j.bios.2016.10.035
23. Li, D. D., Chen, X. C., Ren, K. F., & Ji, J. (2015). Cucurbit[8]uril-based stimuli-responsive films as a sacrificial layer for preparation of free-standing thin films. *Chemical Communications*, *51*(9), 1576–1578. https://doi.org/10.1039/c4cc07899c
24. Richardson, J. J., Bjornmalm, M., & Caruso, F. (2015). Technology-driven layer-by-layer assembly of nanofilms. *Science*, *348*(6233), aaa2491–aaa2491. https://doi.org/10.1126/science.aaa2491
25. Zhong, Y., Li, B., & Haynie, D. T. (2006). Fine Tuning of Physical Properties of Designed Polypeptide Multilayer Films by Control of pH. *Biotechnol. Prog.*, *22*(1), 126–132. https://doi.org/10.1021/bp050130h
26. Shukla, A., Avadhany, S. N., Fang, J. C., & Hammond, P. T. (2010). Tunable Vancomycin Releasing Surfaces for Biomedical Applications. *Small*, *6*(21), 2392–2404. https://doi.org/10.1002/smll.201001150
27. Li, S., Liu, Y. Y., Liu, L. J., & Hu, Q. X. (2016). A Versatile Method for Fabricating Tissue Engineering Scaffolds with a Three-Dimensional Channel for Prevasculature Networks. *ACS Applied Materials and Interfaces*, *8*(38), 25096–25103. https://doi.org/10.1021/acsami.6b07725
28. Custo, C. A., Reis, R. L., & Mano, F. (2016). Photo-Cross-Linked Laminarin-Based Hydrogels for Biomedical Applications. *Biomacromolecules*, *17*(5), 1602−1609. https://doi.org/10.1021/acs.biomac.5b01736
29. Liu, Y., & Hsu, S.-H. (2018). Synthesis and Biomedical Applications of Self-healing Hydrogels. *Frontiers in Chemistry*, *6*, 449. https://doi.org/10.3389/fchem.2018.00449
30. Dababneh, A. B., & Ozbolat, I. T. (2014). Bioprinting Technology: A Current State-of-the-Art Review. *Journal of Manufacturing Science and Engineering, Transactions of the ASME*, *136*(6). https://doi.org/10.1115/1.4028512
31. Chia, H. N., & Wu, B. M. (2015). Recent advances in 3D printing of biomaterials. *Journal of Biological Engineering*, *9*(4). https://doi.org/10.1186/s13036-015-0001-4
32. C-Y Chung, J., & Shum-Tim, D. (2012). Neovascularization in Tissue Engineering. *Cells*, *1*,

1246–1260. https://doi.org/10.3390/cells1041246

33. Chen, D. X. B. (2019). *Bioprinting Vascular Networks in Scaffolds. In: Extrusion Bioprinting of Scaffolds for Tissue Engineering Applications*. Springer, Cham. https://doi.org/10.1007/978-3-030-03460-3_7
34. Jia, W., Gungor-Ozkerim, P. S., Zhang, Y. S., Yue, K., Zhu, K., Liu, W., Pi, Q., Byambaa, B., Dokmeci, M. R., Shin, S. R., & Khademhosseini, A. (2016). Direct 3D bioprinting of perfusable vascular constructs using a blend bioink. *Biomaterials*, *106*, 58–68. https://doi.org/10.1016/j.biomaterials.2016.07.038
35. Tocchio, A., Tamplenizza, M., Martello, F., Gerges, I., Rossi, E., Argentiere, S., Rodighiero, S., Zhao, W., Milani, P., & Lenardi, C. (2015). Versatile fabrication of vascularizable scaffolds for large tissue engineering in bioreactor. *Biomaterials*, *45*, 124–131. https://doi.org/10.1016/j.biomaterials.2014.12.031
36. Pereira, R. F., & Bártolo, P. J. (2015, March 1). 3D Photo-Fabrication for Tissue Engineering and Drug Delivery. *Engineering*. Elsevier Ltd. https://doi.org/10.15302/J-ENG-2015015
37. Ma, J., Wang, Y., & Liu, J. (2018). Bioprinting of 3D tissues/organs combined with microfluidics. *RSC Advances*. Royal Society of Chemistry. https://doi.org/10.1039/c8ra03022g
38. Liew, A. W. L., & Zhang, Y. (2017). In vitro pre-vascularization strategies for tissue engineered constructs–Bioprinting and others. *International Journal of Bioprinting*, *3*(1), 3–17. https://doi.org/10.18063/IJB.2017.01.008.
39. Mandrycky, C., Wang, Z., Kim, K., & Kim, D. H. (2016, July 1). 3D bioprinting for engineering complex tissues. *Biotechnology Advances*. Elsevier Inc. https://doi.org/10.1016/j.biotechadv.2015.12.011
40. Cui, X., & Boland, T. (2009). Human microvasculature fabrication using thermal inkjet printing technology. *Biomaterials*, *30*(31), 6221–6227. https://doi.org/10.1016/j.biomaterials.2009.07.056
41. Gudapati, H., Dey, M., & Ozbolat, I. (2016). A comprehensive review on droplet-based bioprinting: Past, present and future. *Biomaterials*. https://doi.org/10.1016/j.biomaterials.2016.06.012
42. Correia, C. R., Sher, P., Reis, R. L., & Mano, J. F. (2013). Liquified chitosan-alginate multilayer capsules incorporating poly(l-lactic acid) microparticles as cell carriers. *Soft Matter*, *9*(7), 2125–2130. https://doi.org/10.1039/c2sm26784e
43. Caridade, S. G., Monge, C., Gilde, F., Boudou, T., Mano, J. F., & Picart, C. (2013). Free-standing polyelectrolyte membranes made of chitosan and alginate. *Biomacromolecules*, *14*(5), 1653–1660. https://doi.org/10.1021/bm400314s

44. Huang, J., Li, Z., Hu, Q., Chen, G., Ren, Y., Wu, X., & Ren, J. (2018). Bioinspired Anti-digestive Hydrogels Selected by a Simulated Gut Microfluidic Chip for Closing Gastrointestinal Fistula. *iScience*, *8*, 40–48. https://doi.org/10.1016/J.ISCI.2018.09.011

45. Freeman, F. E., & Kelly, D. J. (2017). Tuning Alginate Bioink Stifness and Composition for Controlled Growth Factor Delivery and to Spatially Direct MSC Fate within Bioprinted Tissues, *7*(1), 17042. https://doi.org/10.1038/s41598-017-17286-1

46. Drury, J. L., Dennis, R. G., & Mooney, D. J. (2004). The tensile properties of alginate hydrogels. *Biomaterials*, *25*(16), 3187–3199. https://doi.org/10.1016/j.biomaterials.2003.10.002

47. Marx, K. A. (2003, September). Quartz crystal microbalance: A useful tool for studying thin polymer films and complex biomolecular systems at the solution - Surface interface. *Biomacromolecules*. https://doi.org/10.1021/bm020116i

Chapter 5 – Final remarks and future perspectives

Chapter 5 – Final remarks and future perspectives

The last decade has brought up several approaches to engineer advanced functional constructs to replace damaged tissues and/or organs. The prevascularization of a functional engineered construct prior to its implantation in the human body remains as one of the major challenges in the tissue engineering and regenerative medicine field. Although, the successful replication of the complex native vascular microenvironment has yet to be achieved, simple vascular networks have been already formulated, showing great potential to be used in the near future.

The main goal of this dissertation was to design and develop 3D functional structures to be used in vascular tissue engineering. Those structures encompass natural-origin polymers and have been developed through combination of the LbL assembly technology and hydrogel network formation. To accomplish this, two marine-origin polymers have been used to fabricate the LbL membrane, namely, CHI and ALG or ALG-RGD, and the hydrogel has been produced using xanthan gum.

In order to demonstrate the spatial versatility of the bioprinting technique, different shaped and sized structures were produced. The ALG ink used proved to be successful to replicate the designed ALG structures and to sustain its printed shape after being crosslinked. The multilayered membranes, assembled on top of the ALG printed structures, were obtained using the dip-assisted methodology. The developed LbL membranes encompassed 6 bilayers of CHI/ALG or CHI/ALG-RGD, *i.e.* $(CHI/ALG)_6$ and $(CHI/ALG\text{-}RGD)_6$, respectively.

The ALG printed shapes enveloped in the multilayered membranes were embedded in a xanthan gum solution, with xanthan gum previously chemically modified with glycidyl methacrylate. With the goal of assessing the relevance of the membranes' presence, some hydrogels were constructed with ALG printed shapes that did not have a multilayered membrane (control). Following their reticulation by UV light exposure, the hydrogels containing the ALG printed structures were immersed in an EDTA solution. This solution liquifies the ALG printed shape, leading to a hollow channel within the hydrogel.

In this thesis, HUVECs were injected into these hollow channels, encompassing the multilayered membrane, and the cell adhesion was assessed after 24 hours of culture. The cells showed higher adhesion to the membranes assembled with the ALG-RGD, as revealed by fluorescence microscopy and DNA quantification. It was also verified a significant

amount of non-adhered cells within the channel, likely due to the culture being performed in static conditions.

The presence of the LbL membrane emulates the physical barrier of the capillaries, that separates the blood from the rest of the tissues. As future work, it would be interesting to evaluate cellular behavior at a longer period of time and in a co-culture, to assess the development of two different cell types separated by a multilayered membrane, as well as to perform the cell culture in dynamic conditions. As it is possible to entrap bioactive compounds in-between the LbL membrane, that would be slowly released into the surrounding environment in a sustained and controlled manner, it is possible to use it as a slow-release mechanism of molecules that influence the cellular development and differentiation. The bioactive compounds include signaling peptides, growth factors, and drugs whose release and availability in the hydrogel could be triggered by various release systems.

As aforementioned, the multilayered membranes were assembled using marine-origin polymers, however the LbL assembly technique is not limited to these materials which also contributes to the control of the microenvironment within and outside of the channel. The LbL assembly technology enables the membrane to have the first and last layers made of different materials which means it is possible to functionalize each side of the membrane for a different end goal (*e.g.*, functionalize each side with different materials to promote the binding of different cells or materials). The device developed during this work holds great potential to be scaled-up through several practical ways which is not possible for several devices already in use in tissue engineering applications.

The developed structure could also be applied as a reservoir for cells as the channels is encased by hydrogel, a highly porous network. It allows for solutions exterior to the hydrogel to diffuse to it, reaching the cells within the channel. In addition, the device here studied might have some application as a microfluidics device, however it would be needed to study the hydrogel resistance to the constant flow of solutions.

As the bioprinting technique is a relatively new concept, it is still very dependent on the technology available today. As the new discoveries are made new possibilities come to light like more accurate bioprinters or the ability to bioprint more complex and personalized designs as computed tomography scans.

In conclusion, the fields of tissue engineering and regenerative medicine are in continuous development with new ideas being studied every day by the scientific community. The concept of combining already studied prevascularization techniques has

grown, however the combination here explored has not been reported in literature and has demonstrated its potential to be employed in several ways in the near future.